Biot's Variational Method to determine the thermal strain in layered glazings

Biot's Variational Method to determine the thermal strain in layered glazings

Laura GALUPPI[1] and Gianni ROYER-CARFAGNI[*1,2]

[1]Department of Engineering and Architecture, University of Parma, Parco Area delle Scienze 181/A, I-43124 Parma, Italy

[2]Construction Technologies Institute - Italian National Research Council (ITC-CNR), Via Lombardia 49, I-20098 San Giuliano Milanese, Milano, Italy

Abstract

A critical issue in the structural design of glazed surfaces is the evaluation of the strain consequent to temperature variations due to environmental actions such as solar radiation, which represents one of the main causes of breakage. In the practice, approximate solutions are used, where the temperature profile across the glass thickness is constant or linear, but the consequent thermal stress cannot be adequately estimated from these. On the other hand, sophisticated thermal software is available only for important tasks.

Here, we propose a semi-analytical approach, easily implementable in a simple FEM code, to evaluate the time-dependent temperature profile through the thickness of layered glazing, which is based on the variational method proposed by Biot in the Fifties. A prompt evaluation not only of the temperature field, but also of the heat flux, can be obtained. Compared to other numerical approaches, this method rigorously accounts for energy conservation and, since it does not involve temperature gradients in the formulation, it is particularly efficient for problems with steep temperature variations. Temperature profiles that are not necessarily linear can be approximated by Hermite splines, for a precise evaluation of the thermally-induced stress. Comparisons with a direct numerical solution of the heat-conduction differential equations confirm the accuracy and the effectiveness of the proposed approach.

KEYWORDS: Glazing; variational principle; heat transfer; transient problem; thermal strain.

[*]Corresponding author. *Email address*: gianni.royer@unipr.it

Contents

1 Introduction

The use of glass in transparent envelopes and façades of prestigious buildings has been constantly increasing. This industrialized use of glass is relatively recent if compared to more traditional materials such as timber, steel, concrete or masonry, but requires particular attention due to its intrinsic brittleness [26, 16]. The design has to consider not only the self-weight and service loads, but also the effects of the surrounding environment. A key aspect, unfortunately often overlooked in the practice, consists in the evaluation of the thermal stress due to temperature variations induced by climatic changes because, indeed, this is the most experienced cause of breakage [53, 48, 27]. This is why the precise evaluation of the temperature field inside the glass pane consequent to variable environmental conditions is of paramount importance to glass designers and manufacturers.

The temperature field in the glazing depends upon a large number of environmental and geometric parameters, such as internal/external temperatures, solar radiance, material thermal properties, shadowed portions [58, 24], pane inclination [46, 22]. Structural engineers are usually not familiar with the use of sophisticated thermal software and, on the other hand, the actual boundary conditions are affected by uncertainties. This is why, the common design practice relies upon codes and standards [1, 3], which provide simplified formulas to evaluate the temperature distribution in the glazing. There should be some caution in using these formulations because the assumptions on which they are based are practically never described in background documents. Consequently, the regulatory recommendations, and the software which implements them, are black boxes to which the designer must submit. The authors have recently [30] reviewed existing methods proposed in standards and proposed an comprehensive engineering method for the evaluation of the temperature field, but this is based on strong simplifying hypotheses and applies to single glazing only.

Substantial research is dedicated to the analysis of the heat exchange phenomena in glazing, but this has been mainly addressed towards determining the *overall* thermal transmittance of the unit [60, 43]. On the other hand, what is important for the integrity of glass is a precise determination of the temperature profile inside the glazing, from which the thermal strain and, hence, the thermal stress, can be readily estimated. Most of the proposed methods rely on the assumption of *thermally thin* glass panels, where the temperature is considered to be uniform in-the-thickness, while the most refined approaches assume a linear trend. These hypotheses are usually consistent when evaluating the insulating properties of the glazing, but the associated thermal strain is compatible, i.e., in an isolated plate it does not give raise to thermal-induced eigenstresses [32]. The situation is more complicated in laminated and layered glass panes, where the temperature profile in the direction of the thickness is strongly influenced by the presence of coating(s) and interlayer(s) foil(s) [9, 49, 12]. The aforementioned approximations roughly interpret the spatial dependence of the temperature field, which is the source of stress. Very accurate estimates

of the temperature field in architectural glazings are obtained, by specialized engineers, by solving the governing equations with finite difference techniques, in both space and time [36, 9, 54], or by using sophisticated Finite Element codes, but this can be realistically done only for the most important projects. What is needed is a reliable simplified method to be used for the structural verification.

Analytical methods of solution for heat conduction problems have received considerable attention from the Fifties to the Eighties [38, 59, 15], but they are now abandoned due to the massive use of numerical codes. Here, we propose a method to evaluate the time-dependent temperature distribution across the thickness of layered glazing, which is based on the ingenious variational method proposed by Biot [13, 14]. This provides a very effective weak formulation of the heat conduction equation, which is now specialized to the one-dimensional problem of multilayer laminated glass. A semi-analytical method of solution, where each layer composing the panel is regarded as a 1-dimensional element, can be obtained by approximating the relevant fields with Hermite splines, combining optimal localization and excellent approximation power [23, 25, 51]. The resulting algebraic system of linear equations can be solved numerically or, more in general, the whole method can be implemented in a simple FEM software.

From a theoretical point of view, the matrix formulation presents a strong analogy with the equation governing the Lagrangian mechanics for the slow motion of a dissipative system with negligible inertia forces. Indeed, Biot's Variational Method (BVM) treats the energy balance as a holonomic constraint, which is rigorously satisfied also in the numerical approximation. Another great advantage is that no temperature gradients are involved in the weak form of the governing equations: in this way, it is possible to consider problems involving steep variation of the temperature profile with no need of a very fine mesh, as instead is the case in the most used FEM approaches. The shape functions are smooth, whereas in other methods they are assumed piecewise linear, but the irregularity spoils the evaluation of the thermally-induced stress field. Moreover, this approach allows a prompt evaluation not only of the temperature field, but also of the heat flux.

To illustrate both accuracy and computational efficiency, the proposed method is applied to monolithic and laminated glass elements. First, the simplest case of constant environmental conditions is considered, in order to evaluate the time needed to reach the steady state. Successively, the transient response is analyzed under daily variations of the boundary conditions, according to standard environmental and climate parameters. The obtained results are compared with a direct numerical solution of the heat-conduction partial differential equation, which however necessitates of a much higher numerical effort. Results are found in excellent agreement.

2 The thermoelastic problem for layered panes

The considered model problem is that of a layered glazing pane, representing the component of a façade. The pane is composed of an arbitrary number N of layers of thickness s_i, $i = 1, \ldots, N$, made of different materials characterized by different physical and thermal properties (mass per unit volume, specific heat, thermal conductivity, emissivity, reflectivity, absorptivity and transmissivity with respect to the solar radiation). Although the theory is developed in general, the practical case is certainly represented by laminated glass, for which the layers are the glass plies and the polymeric interlayers. In general the thermal properties of the glass plies can differ one another within the same laminated package.

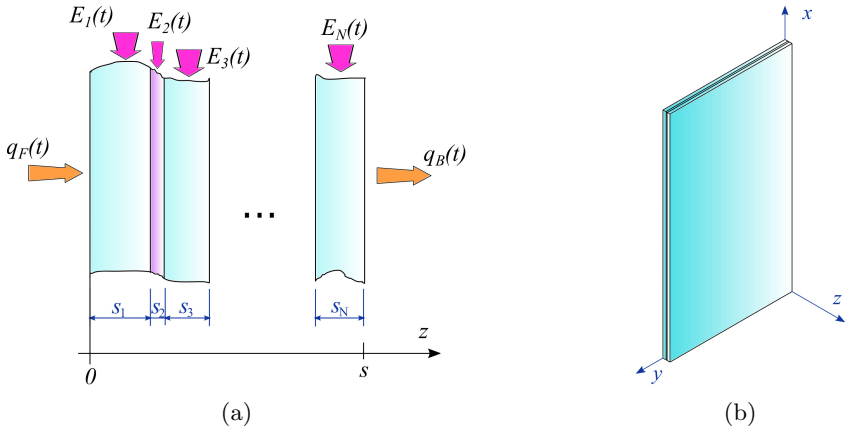

Figure 1: a) Scheme of the laminated package and b) reference system.

The thermoelastic problem is uncoupled [17, 19], i.e., the temperature distribution is not affected by the stress and displacement fields and, hence, it is determined by the heat transfer equations only. The state of stress is found "in cascade", by considering the thermal strain as an applied action, varying with time.

Consider the reference frame (x, y, z) of Figure 1(b), with the x, y axes parallel to surface of the panel, and the z axis at right angle to that. The "front" surface, in contact with the external environment, is that at $z = 0$, while the "back" indoor surface is at $z = s$, where $s = \sum_{i=1}^{N} s_i$ is the total thickness of the pane. Thermal energy can be stored in each layer, according to the heat capacity; heat exchange is regulated by convection with internal and external air and radiation from environmental source. In the simplest case, the heat conduction with frames or shadowed parts of the panel at different temperature is not considered, while the panel is assumed to be large in the x and y directions in comparison to its thickness in the z direction. From these hypotheses, a 1-D version of the problem can be formulated, in which the temperature field depends only on the z coordinate and on time.

2.1 The boundary value problem in heat transfer

Let $T_{ext}(t)$ and $T_{int}(t)$ denote the absolute temperatures of the external and internal environment, respectively. In general, $T_{ext}(t)$ undergoes daily and seasonal fluctuations according to the location, whereas $T_{int}(t)$ is much more stable, and can be considered almost constant in the calculation.

Heat convection is regulated by the convective heat transfer coefficients with the internal and external environment, respectively denoted by h_{iC} and h_{eC}, whose standard values are provided by Standards [4, 6]. The external surface is irradiated by the sky vault, which is treated as large enclosure surface, at an absolute temperature $T_{sky}(t)$ [1, 56], while the internal surface are irradiated by the inner-room surfaces at $T_{int}(t)$ [1, 44]. The exchanged *radiant energy* depends upon the difference of the forth powers of the absolute temperatures of the involved surfaces [40], but if the temperature difference is small with respect to their mean value, a linear dependence can be conveniently assumed according to the radiation heat transfer coefficients, here indicated as h_{iR} and h_{eR} for the internal and external heat exchange, respectively. If $T_F(t)$ and $T_B(t)$ are the absolute temperatures of the front and the back surfaces of the pane, respectively, one can write

$$h_{eR} = 4\varepsilon\sigma \left[\frac{T_{sky}(t) + T_F(t)}{2}\right]^3 , \qquad h_{iR} = 4\varepsilon\sigma \left[\frac{T_{int}(t) + T_B(t)}{2}\right]^3 . \tag{2.1}$$

These coefficients are time-dependent, but since the daily change in temperature is of the order of 20 K, their variation is small. This is why, as also suggested by standards [6, 3], in the engineering practice both h_{eR} and h_{iR} are provided as fixed conventional values[1].

In conclusion, the heat fluxes $q_F(t)$ and $q_B(t)$ though the front and back surfaces of the pane, respectively, take the form

$$q_F(t) = h_{eC}\left[T_{ext}(t) - T_F(t)\right] + h_{eR}\left[T_{sky}(t) - T_F(t)\right] = h_e\left[\tilde{T}_{ext}(t) - T_F(t)\right] , \tag{2.2a}$$

$$q_B(t) = (h_{iC} + h_{iR})\left[T_B(t) - T_{int}(t)\right] = h_i\left[T_B(t) - T_{int}(t)\right] , \tag{2.2b}$$

where $h_i = h_{iC} + h_{iR}$ and $h_e = h_{eC} + h_{eR}$ are the *total* heat transfer coefficients (accounting for convection and infra-red radiation), whereas

$$\tilde{T}_{ext}(t) = \frac{h_{eC}T_{ext}(t) + h_{eR}T_{sky}(t)}{h_e} \tag{2.3}$$

[1]It should be mentioned that the *general method* proposed by [3] suggests that, for a refined calculation, the dependence on the time-varying temperatures of h_{eR} and h_{iR} should be considered: their values is found via an iterative calculations, by updating the values at each iteration until convergence.

is a *fictitious* temperature, accounting for the heat flow from the external environment.

In addition, the pane is hit by the solar radiation $G(t)$, whose intensity depends on various factors (presence of shadows [58, 24], season, façade orientation, geographic location, time of day, panel inclination [46, 22]). This is absorbed in the volume of the layers, as schematically indicated in Figure 1(a).

2.2 Thermal equations

With reference to Figure 1(a), a set of local non-dimensional coordinates

$$\zeta_i := \frac{z - \sum_{k=1}^{i-1} s_k}{s_i} \tag{2.4}$$

is defined, so that $\zeta_i \in [0,1]$ for the $i-$th ply, $i = 1, \ldots, N$. The temperature field is described by the functions $T_i(\zeta_i, t)$.

A part of the energy $G(t)$ associated with the solar radiation is absorbed, another part is reflected and the remain part is transmitted: each layer is characterized by the absorptivity α_i, the reflectivity r_i and the transmissivity τ_i, $i = 1 \ldots N$. The solar energy hitting the i-th layer is $\overline{\tau}_i G(t)$, where

$$\overline{\tau}_i := \begin{cases} 1 \quad \text{for } i = 1\,, \\ \prod_{k=1}^{i-1} \tau_k \quad \text{for } i = 2, \ldots, N\,. \end{cases} \tag{2.5}$$

Due to absorption, the solar radiation is attenuated, i.e., the "available" energy decreases along the thickness, depending on the *extinction coefficient* p_i of the material. According to the Bouguer-Beer-Lambert law [40, 34], the absorbed energy $E_i(\zeta_i, t)$ at the generic local coordinate ζ_i is given by [10, 36, 49]

$$E_i(\zeta_i, t) = \left(1 - e^{-p_i s_i \zeta_i}\right)\ \overline{\tau}_i\ G(t)\,. \tag{2.6}$$

Obviously, the material absorptivity α_i, corresponding to the part absorbed in the whole layer, corresponds to $E_i(1,t)$ and reads [40] $\alpha_i = 1 - e^{-p_i s_i}$. However, a common approximation [60], which will be used here, consists in assuming a linear dependence in the thickness of the layer, in the form

$$E_i(\zeta_i, t) = \alpha_i\ \zeta_i\ \overline{\tau}_i\ G(t)\,. \tag{2.7}$$

Following [34], this is acceptable for laminated glass, since the thickness of the plies is so small that the crossing radiation is only mildly attenuated. The approximation (2.7)

can also be used for the polymeric interlayers, taking into account that their absorption coefficient and thickness is much smaller than that of glass.

The 1-D heat-conduction equation for the $i-$th ply reads [40]

$$\rho_i c_{p;i} \frac{\partial T_i(\zeta_i,t)}{\partial t} = \frac{\lambda_i}{s_i^2} \frac{\partial^2 T_i(\zeta_i,t)}{\partial \zeta_i^2} + \frac{1}{s_i} \frac{\partial E_i(\zeta_i,t)}{\partial \zeta_i} \,, \tag{2.8}$$

where ρ_i, $c_{p;i}$ and λ_i respectively denote the mass per unit volume, the specific heat and the thermal conductivity of the $i-$th ply. The term on the l.h.s. of (2.8) represents the heat storage in the glass element, whereas on the r.h.s. one finds the heat conduction and the contribution of the solar radiation. Observe that $\frac{1}{s_i}\frac{dE_i(\zeta_i)}{d\zeta_i}$ represents the absorbed solar radiation per unit thickness per unit time [10, 36, 34], which is constant if (2.7) is used.

The boundary conditions for the front and back surfaces, in contact with the external and internal environments, are of the third (Robin) kind, i.e.,

$$-\frac{\lambda_1}{s_1} \left. \frac{\partial T_1(\zeta_1,t)}{\partial \zeta_1} \right|_{\zeta_1=0} = h_e \left[\tilde{T}_{ext}(t) - T_F(t) \right] \,, \tag{2.9a}$$

$$-\frac{\lambda_N}{s_N} \left. \frac{\partial T_n(\zeta_N,t)}{\partial \zeta_N} \right|_{\zeta_N=1} = h_i \left[T_B(t) - T_{int}(t) \right] \,. \tag{2.9b}$$

At the interfaces between adjacent plies both the temperature field and the heat conduction flux must be continuous [9], that is

$$T_i(\zeta_i,t)|_{\zeta_i=1} = T_{i+1}(\zeta_{i+1},t)|_{\zeta_{i+1}=0} \,, \tag{2.10a}$$

$$-\frac{\lambda_i}{s_i} \left. \frac{\partial T_i(\zeta_i,t)}{\partial \zeta_i} \right|_{\zeta_i=1} = -\frac{\lambda_{i+1}}{s_{i+1}} \left. \frac{\partial T_{i+1}(\zeta_{i+1},t)}{\partial \zeta_{i+1}} \right|_{\zeta_{i+1}=0} \,, \; i=1,\dots,N-1 \,. \tag{2.10b}$$

The second of (2.10) implies that, at the interfaces, the spatial derivative of the left and right temperature fields are not equal, being related by the ratio between the thermal conductivities of the two materials.

An approximate solution can be found by neglecting the heat storage, represented by the term $\frac{\partial T_i(\zeta_i,t)}{\partial t}$ in (2.8), which corresponds to the *steady state* in which the energies flowing inwards and outwards are equal and no heat is stored. This can occur only in the (unrealistic) case where the external temperatures $T_{ext}(t)$, $T_{sky}(t)$, and the solar radiation $G(t)$ are constant in time. More in general, this thermal equilibrium can be reached when the time-scale of the environmental conditions is much higher than the time required to reach steady-state condition, but, as discussed in [30], this is not the case for architectural

glazing. In fact, the time required to reach the steady state temperature is usually of the order of one hour, but the solar radiance and the external temperature can substantially vary in a similar time interval.

The solution for the steady state is quite simple and provides that the temperature field is piecewise parabolic. At the i-th interface, the first spatial derivative of the temperature distribution are inversely proportional to the ratio between the thermal conductivities of the two materials[2], as per $(2.10)_2$.

2.3 Temperature-induced state of stress

In order to apply the equation of elasticity, we will refer to the physical coordinate z of Figure 1(b), instead of the normalized coordinate ζ. Let $\Delta T(z)$ be the temperature variation and denote by α_T the thermal expansion coefficient of the material. Denoting by $\mathbf{I}$ the identity tensor, the thermal strain tensor $\boldsymbol{\varepsilon}_T$ is given by

$$\boldsymbol{\varepsilon}_T = \alpha_T \Delta T(z) \mathbf{I} \,. \tag{2.11}$$

The stress tensor reads $\boldsymbol{\sigma}$

$$\boldsymbol{\sigma} = \mathbb{C} \left(\boldsymbol{\varepsilon} - \boldsymbol{\varepsilon}_T \right) \,, \tag{2.12}$$

where $\mathbb{C}$ is the elasticity tensor and $\boldsymbol{\varepsilon}$ is the strain tensor, which shall satisfy the compatibility conditions. Once $\boldsymbol{\varepsilon}_T$ is known, the state of stress can be determined using any commercial FEM code.

For a qualitative analysis, it is instructive to consider the simplest case of a monolithic plate ($N = 1$), undergoing a given in-the-thickness temperature variation with respect to the reference value. For a plate that can in-plane freely expand or contract, the elastic solution can be found by superposition [32]. First the plate is fictitiously constrained at its edges in the (x, y) directions: the in-plane stress consequent to the thermal variation is uniform and equi-biaxial at each level $z = const$ and reads [42]

$$\sigma_x = \sigma_y = -\frac{\alpha_T E}{1 - \nu} \, \Delta T(z) \,, \tag{2.13}$$

where E and ν are the Young's modulus and the Poisson's coefficient, respectively. The constrain reactions are orthogonal to the border, so to equilibrate the state of stress (2.13).

[2] More precisely, $\frac{\partial T_i(\zeta_i, t)}{\partial \zeta_i}$ and $\frac{\partial T_{i+1}(\zeta_{i+1}, t)}{\partial \zeta_{i+1}}$ are inversely proportional to the ratio of the thermal conductivities per unit thickness λ/s of the two materials. The first derivatives with respect to z are instead inversely proportional to the ratio of the thermal conductivities λ of the two materials.

Since the real plate is not constrained, one has thus to superimpose to this state of stress the one obtained by applying to the plate the constrain reactions with opposite signs. It can be directly verified [27] that, when $\Delta T(z)$ is either constant or linearly varying along the plate thickness, the stress distribution due to these is opposite to that given by (2.13), providing a null total stress. This is because the thermal strain tensor $\boldsymbol{\varepsilon}_T$ fulfills the compatibility relations and, hence, both equilibrium and compatibility are satisfied when the plate is in a stress free state, with $\boldsymbol{\varepsilon} = \boldsymbol{\varepsilon}_T$ and $\boldsymbol{\sigma} = \mathbf{0}$. Of course, the plate expand and/or inflects due to the non-null strain.

When the temperature variation is not a linear function of z, $\boldsymbol{\varepsilon}_T$ does not satisfy the compatibility relations. In this case, the thermal stress is not nil. It is worth mentioning that, when analyzing the thermal profiles through glazed surfaces, it is customary to approximate the temperature field as linearly varying along the panel thickness: the thermally-induced stress cannot be determined from this. If one is interested in evaluating the possible risks of rupture due to thermal gradients, it is therefore necessary to consider a more refined model to determine the temperature field. This is particularly important for laminates, where the layer-wise mismatch of thermal and elastic properties can induce stress concentrations [33, 28].

3 Application of Biot's Variational principle

The ingenious variational approach proposed by Biot [13, 14] can be applied to solve the complete thermal analysis through the definition of spatial shape functions for the temperature field. Here the method is extended to the case of multi-layered domains.

3.1 The variational approach for layered elements

Before passing to the specialization for a layered pane, it is useful to recall Biot's variational principle in general terms, for a homogeneous body of density ρ, with specific heat c_p and conductivity λ. The principle is stated in terms of the heat flow vector field $\mathbf{H}$, also referred to as *heat displacement*, whose time rate of change $\dot{\mathbf{H}}$ is the heat flux across an area normal to $\dot{\mathbf{H}}$. For an arbitrary volume V with surface S and outer normal $\mathbf{n}$, conservation of energy provides

$$\int_V \mathbf{H}\cdot\mathbf{n}\,dV = -\int_S \rho c_p T\,dS \;\Rightarrow\; -\rho c_p T = \nabla\cdot\mathbf{H}\,, \tag{3.1}$$

where T is the temperature field above equilibrium temperature. Notice that this relation does not involve any time derivative, and it may be regarded as a holonomic constraint in the sense of classical mechanics. As remarked in [14], the temperature and the heat displacement are conjugate variables, analogue to force and displacement in classical mechanics.

The variational principle can be stated as

$$\delta\mathcal{V} + \delta\mathcal{D} = -\int_S T\delta\mathbf{H}\cdot\mathbf{n}\,dS\,, \tag{3.2}$$

where

$$\mathcal{V} = \frac{\rho c_p}{2}\int_V T^2 dV\,, \tag{3.3a}$$

$$\delta\mathcal{D} = \frac{1}{\lambda}\int_V \dot{\mathbf{H}}\cdot\delta\mathbf{H}\,dV\,. \tag{3.3b}$$

Here $\mathcal{V}$ is the *thermal potential* which is related to the thermal energy of the system, whereas the *dissipation function* $\mathcal{D}$ equals the production of entropy in the system. The variation of the thermal potential $\mathcal{V}$, together with the conservation of energy (3.1), yields

$$\delta\mathcal{V} = \rho c_p\int_V T\delta T\,dV = -\int_S T\delta\mathbf{H}\cdot\mathbf{n}\,dS + \int_V \delta\mathbf{H}\cdot\nabla T\,dV\,, \tag{3.4}$$

so that the variational principle (3.2) leads

$$\int_V \left[\nabla T + (1/\lambda)\dot{\mathbf{H}}\right]\cdot\delta\mathbf{H}\,dV = 0\,. \tag{3.5}$$

For an arbitrary variation $\delta\mathbf{H}$, this reduces to the heat conduction equation

$$\lambda\nabla T + \dot{\mathbf{H}} = 0\,. \tag{3.6}$$

Taking the divergence on both side, and recalling (3.1), one obtains the equation

$$\lambda(\nabla\cdot\nabla T) = \rho c_p\dot{T}. \tag{3.7}$$

It is important to note that the heat displacement cannot be completely evaluated from the variational principle, since this involves only its time derivative, i.e., the heat flux. The heat displacement can be determined up to an additive function, which depends upon the boundary conditions. This indeterminacy, though inessential, is congenital in Biot's variational principle. Indeed, in the general derivation leading to (3.7) from (3.6), the addition of a time-independent solenoidal vector field to the heat displacement $\mathbf{H}$ would provide the same result.

We now pass to the problem of the layered pane. The 1D equation are set in terms of the local coordinates ζ_i defined in (2.4), for which it is important to recall that $s_i \frac{\partial}{\partial \zeta_i} = \frac{\partial}{\partial z}$. Moreover, the heat displacement is now represented by the scalar variable $\mathcal{H}$, whose time rate $\dot{\mathcal{H}}$ indicates the heat flux in the positive direction of the axis z. It is convenient to specify this field for the $i-$th layer, $i = 1 \dots N$, as $\mathcal{H}_i = \mathcal{H}_i(\zeta_i, t)$, defined for $\zeta_i \in [0, 1]$.

For the $i-$th layer the conservation of energy, i.e., the counterpart of (3.1), reads

$$\frac{\partial \mathcal{H}_i(\zeta_i, t)}{\partial \zeta_i} = -\rho_i c_{p;i} s_i \; T_i(\zeta_i, t) \, . \tag{3.8}$$

Following (3.3), for the $i-$th layer one defines the thermal potential $\mathcal{V}_i$ and the dissipation function $\mathcal{D}_i$ as

$$\mathcal{V}_i = \frac{\rho_i c_{p;i} s_i}{2} \int_0^1 T_i^2(\zeta_i, t) \; d\zeta_i \, , \tag{3.9a}$$

$$\delta \mathcal{D}_i = \frac{s_i}{\lambda_i} \int_0^1 \dot{\mathcal{H}}_i(\zeta_i, t) \delta \mathcal{H}_i(\zeta_i, t) \; d\zeta_i \, . \tag{3.9b}$$

Considering the variation of the temperature field and of the heat displacement field, related by the olonomic constrain (3.8), the first variation of the thermal potential $\mathcal{V}_i$ can be written as

$$\delta \mathcal{V}_i = \rho_i c_{p;i} s_i \int_0^1 T_i \delta T_i \; d\zeta_i = - \int_0^1 T_i \frac{\partial}{\partial \zeta_i} \delta \mathcal{H}_i \; d\zeta_i = - \Big[T_i \delta \mathcal{H}_i \Big]_0^1 + \int_0^1 \frac{\partial T_i}{\partial \zeta_i} \delta \mathcal{H}_i \; d\zeta_i \, , \tag{3.10}$$

where, here and further, the dependence of T_i and $\mathcal{H}_i$ on ζ_i and t is omitted for brevity. With respect to (3.4), one should notice that the domain where the integrals are evaluated is not represented by an arbitrary volume V, but by the whole layer. This choice is dictated by the form of the shape functions through which the temperature and heat displacement fields will be approximated.

In order to consider the fact that there are *heat sources* in the system, following [14] the additional fields $\mathcal{H}_i^*$, $i = 1, \dots, N$, are introduced, which represent the contribution of the absorbed part of the solar radiation. The total heat displacement is hence

$$\overline{\mathcal{H}}_i = \mathcal{H}_i + \mathcal{H}_i^* . \tag{3.11}$$

Recalling that the energy absorbed per unit volume in the $i-$th layer is given by $\partial E_i(\zeta_i, t)/\partial \zeta_i$, with $E_i(\zeta_i, t)$ given by (2.6) or (2.7), this can be written as

$$\frac{\partial \mathcal{H}_i^*}{\partial \zeta_i} = \int_0^t \frac{\partial E_i(\zeta_i, t)}{\partial \zeta_i}\, dt\,. \tag{3.12}$$

The function $E_i(\zeta_i, t)$ is a datum, so that the l.h.s. is assigned. However, as pointed out in [14], this equation does not determine $\mathcal{H}_i^*$ uniquely, but the indeterminacy is inessential since any field satisfying (3.12) can be chosen.

According to [14], the variational principle for the $i-$th layer can be stated as

$$\delta\mathcal{V}_i + \delta\mathcal{D}_i = -\Big[T_i \delta\mathcal{H}_i\Big]_0^1 - \frac{s_i}{\lambda_i}\int_0^1 \dot{\mathcal{H}}_i^*\ \delta\mathcal{H}_i\ d\zeta_i\,, \tag{3.13}$$

where the energy conservation (3.8) plays the role of a holonomic constraint. Following the same arguments leading to (3.5), recalling (3.10) the expression (3.13) provides

$$\delta\mathcal{V}_i + \delta\mathcal{D}_i + [T_i\delta\mathcal{H}_i]_0^1 + \frac{s_i}{\lambda_i}\int_0^1 \dot{\mathcal{H}}_i^*\ \delta\mathcal{H}_i\ d\zeta_i = \int_0^1 \left[\frac{\partial T_i}{\partial \zeta_i} + \frac{s_i}{\lambda_i}\left(\dot{\mathcal{H}}_i + \dot{\mathcal{H}}_i^*\right)\right]\delta\mathcal{H}_i\ d\zeta_i = 0\,. \tag{3.14}$$

Since the variation $\delta\mathcal{H}_i$ is arbitrary, one obtains

$$-\dot{\mathcal{H}}_i = \frac{\lambda_i}{s_i}\frac{\partial T_i}{\partial \zeta_i} + E_i(\zeta_i)\,. \tag{3.15}$$

which corresponds to the heat conduction law (2.8), now written in terms of $\mathcal{H}_i$. This can be directly verified by taking the first derivative with respect to ζ_i and recalling (3.8).

For the whole layered panel, the variational principle may be stated as

$$\delta\mathcal{V} + \delta\mathcal{D} = -\sum_{i=1}^{N}\Big[T_i\delta\mathcal{H}_i\Big]_0^1 - \sum_{i=1}^{N}\frac{s_i}{\lambda_i}\int_0^1 \dot{\mathcal{H}}_i^*\ \delta\mathcal{H}_i\ d\zeta_i\,. \tag{3.16}$$

where $\delta\mathcal{V} = \sum_{i=1}^N \delta\mathcal{V}_i$ and $\delta\mathcal{D} = \sum_{i=1}^N \delta\mathcal{D}_i$. The strength of the variational approach consists in the fact that the relevant fields $\mathcal{H}_i(\zeta_i, t)$, and consequently $T_i(\zeta_i, t)$, can be approximated with shape functions which depend on $\zeta_i \in [0, 1]$ and the associated coefficients, which are a function of time. This procedure is classical in the Finite Element Method (FEM).

Therefore, the whole heat displacement field $\mathcal{H} = \mathcal{H}(z, t)$, which is piecewise defined by the fields $\mathcal{H}_i = \mathcal{H}_i(\zeta_i, t)$, $i = 1, \ldots, N$, can be completely defined by M time-dependent *generalized coordinates* $f_k(t)$, $k = 1, \ldots, M$, defining the field configuration. With a little abuse of notation, one can schematically write

$$\mathcal{H}(z,t) = \sum_{i=1}^{N} \mathcal{H}_i\big(\zeta_i, f_1(t), \dots, f_M(t)\big)\,. \tag{3.17}$$

Hence, the variational principle (3.16) provides [14] a system of M equations, in the form

$$\frac{\partial \mathcal{V}}{\partial f_k} + \frac{\partial \mathcal{D}}{\partial \dot{f}_k} = \mathcal{Q}_k + \mathcal{Q}_k^*\,, \tag{3.18}$$

where

$$\mathcal{D} = \sum_{i=1}^{N} \frac{s_i}{2\,\lambda_i} \int_0^1 \Big[\dot{\mathcal{H}}_i\big(\zeta_i, f_1(t), \dots, f_M(t)\big)\Big]^2 \, d\zeta_i\,, \tag{3.19}$$

is the overall dissipation function. Notice that, since the temperature field is related to the heat displacement by (3.8), also the thermal potential $\mathcal{V}$ depends on the generalized coordinates. In (3.18), $\mathcal{Q}_k$ is the generalized driving force due to the temperature at the boundary and interfaces, while $\mathcal{Q}_k^*$ is the generalized force due to the heat absorbed in the volume element. These are defined as

$$\mathcal{Q}_k := -\sum_{i=1}^{N} \left[T_i \frac{\partial \mathcal{H}_i\big(\zeta_i, f_1(t), \dots, f_M(t)\big)}{\partial f_k} \right]_0^1\,, \tag{3.20a}$$

$$\mathcal{Q}_k^* := -\sum_{i=1}^{N} \frac{s_i}{\lambda_i} \int_0^1 \dot{\mathcal{H}}_i^* \, \frac{\partial \mathcal{H}_i\big(\zeta_i, f_1(t), \dots, f_M(t)\big)}{\partial f_k} \, d\zeta_i\,. \tag{3.20b}$$

Notice that in this variational description the interface conditions (2.10) should be taken into account through compatible shape functions. No continuity conditions are *a priori* required on the heat displacement field.

Biot observed [14] that equations (3.18) are of the same form as those of Lagrangian mechanics for the slow motion of a dissipative system with negligible inertia forces, for which $\mathcal{V}$ corresponds to the potential energy and $\mathcal{D}$ to the dissipation function. The quantities $\mathcal{Q}_k$ and $\mathcal{Q}_k^*$ appearing on the right-hand side represent generalized *thermal driving forces* due to the temperature distribution at the boundary and to heat sources, and defined by a method of virtual work as in mechanics. For this reason, they are referred to as *thermal forces*.

3.2 Formulation à la Biot for layered glazing

By approximating the relevant fields with appropriate shape-functions, the variational principle can be used to define a FEM formulation of the thermal problem.

3.2.1 Shape functions and conformal mesh interfaces

Approximate the heat displacement and temperature fields in the $i-$th layer in the form

$$\mathcal{H}_i(\zeta_i, t) = \mathbf{n}(\zeta_i) \cdot \mathbf{f}_i(t)\,, \tag{3.21a}$$

$$T_i(\zeta_i, t) = -\frac{1}{\rho_i c_{p;i} s_i} \mathbf{p}(\zeta_i) \cdot \mathbf{f}_i(t)\,. \tag{3.21b}$$

Here, $\mathbf{f}_i(t) = [f_{i,1}(t)\ f_{i,2}(t)\ f_{i,3}(t)\ f_{i,4}(t)\ f_{i,5}(t)]^T$ (where ^{T} denotes the transpose) is the vector of the generalized coordinates for the i-th ply, while $\mathbf{n}(\zeta_i)$ and $\mathbf{p}(\zeta_i)$ are vectors of spatial shape functions, defined as Hermite polynomials in the form

$$\mathbf{n}(\zeta_i) = \begin{bmatrix} \zeta_i^4/2 - \zeta_i^3 + \zeta_i - 1/2 \\ -\zeta_i^4/2 + \zeta_i^3 \\ \zeta_i^4/4 - 2\zeta_i^3/3 + \zeta_i^2/2 - 1/12 \\ \zeta_i^4/4 - \zeta_i^3/3 \\ 1 \end{bmatrix}, \qquad \mathbf{p}(\zeta_i) = \frac{d}{d\zeta_i}\mathbf{n}(\zeta_i) = \begin{bmatrix} 2\zeta_i^3 - 3\zeta_i^2 + 1 \\ -2\zeta_i^3 + 3\zeta_i^2 \\ \zeta_i^3 - 2\zeta_i^2 + \zeta_i \\ \zeta_i^3 - \zeta_i^2 \\ 0 \end{bmatrix}. \tag{3.22}$$

Notice that (3.8) is automatically satisfied. Observe as well that the fifth generalized coordinate $f_{i,5}(t)$ is inessential for what concerns the temperature field, but it affects the heat displacement and, hence, the heat flux $\dot{\mathcal{H}}_i(\zeta_i, t) = \mathbf{n_i}(\zeta_i) \cdot \dot{\mathbf{f}}_i(t)$.

The generalized coordinates represent the nodal displacements of finite elements. In fact, each layer composing the pane is regarded as a 1-dimensional element, for which the temperatures and its first spatial derivatives at the boundary $\zeta_i = 0, 1$ correspond to the values of $f_{i,k}(t)$, $k = 1, \ldots, 4$.

The interface conditions (2.10) provide

$$\begin{aligned} &f_{i+1,1}(t) = \beta_{i;i+1} f_{i,2}(t)\,, \\ &f_{i+1,3} = \beta_{i;i+1}\gamma_{i;i+1} f_{i,4}(t)\,,\ i = 1, \ldots, N-1, \end{aligned} \tag{3.23}$$

where we have defined

$$\beta_{i;i+1} = \frac{\rho_{i+1} c_{p;i+1} s_{i+1}}{\rho_i c_{p;i} s_i}\,, \quad \gamma_{i;i+1} = \frac{\lambda_i s_{i+1}}{\lambda_{i+1} s_i}\,. \tag{3.24}$$

These $2(N-1)$ equations represent the conditions for conformity, which reduces to $5N - 2(N-1) = 3N+2$ the number of independent nodal coordinates. The corresponding vector will be denoted by $\mathbf{F}(t)$.

It is convenient to decompose $\mathbf{F}(t)$ in the two subvectors: $\mathbf{F}_T(t)$, with $2N+2$ components defined only by $f_{i,k}(t)$, $k = 1, \dots, 4$, $i = 1, \dots, N$, affecting the temperature field, and the remaining part $\mathbf{F}_H(t)$ with N, related to $f_{i,5}(t)$, $i = 1, \dots, N$, which has an effect on the the heat displacement. Recalling (3.23), these vectors will be defined as

$$\begin{aligned}
&\mathbf{F}(t) := [\mathbf{F}_T(t) | \mathbf{F}_H(t)]^T\,,\\
&\mathbf{F}_T(t) := [f_{1,1}(t), f_{1,2}(t), f_{1,3}(t), f_{1,4}(t), f_{2,2}(t), f_{2,4}(t), \dots, f_{i,2}(t), f_{i,4}(t), \dots, f_{N,2}(t), f_{N,4}(t)]^T\,,\\
&\mathbf{F}_H(t) := [f_{1,5}(t), \dots, f_{N,5}(t)]^T\,.
\end{aligned} \tag{3.25}$$

The vector $\mathbf{F}(t)$ is related to $\mathbf{f}_i(t)$ by

$$\mathbf{f}_i(t) = \mathbf{L}_i\ \mathbf{F}(t)\,, \tag{3.26}$$

where $\mathbf{L}_i$ are $5 \times (3N+2)$ matrices, whose expressions are recorded in the Appendix A.1.

Therefore, the variational principle (3.18) may be written in matrix form[3] as

$$\frac{\partial \mathcal{V}}{\partial \mathbf{F}(t)} + \frac{\partial \mathcal{D}}{\partial \dot{\mathbf{F}}(t)} = \mathbf{Q} + \mathbf{Q}^*\,, \tag{3.27}$$

where, following (3.20), $\mathbf{Q}$ and $\mathbf{Q}^*$ may be evaluated as

$$\mathbf{Q} := -\sum_{i=1}^{N} \left[T_i \frac{\partial \mathcal{H}_i}{\partial \mathbf{F}(t)} \right]_0^1\,, \tag{3.28a}$$

$$\mathbf{Q}^* = -\sum_{i=1}^{N} \frac{s_i}{\lambda_i} \int_0^1 \dot{\mathcal{H}}_i^*\ \frac{\partial \mathcal{H}_i}{\partial \mathbf{F}(t)}\ d\zeta_i\,. \tag{3.28b}$$

Accounting for (3.26), one can write

[3] We define the derivative of a scalar with respect to a column vector as a column vector.

$$\mathcal{H}_i(\zeta_i,t) = [\mathbf{L}_i^T\mathbf{n}(\zeta_i)]\cdot\mathbf{F}(t)\,, \tag{3.29a}$$
$$\dot{\mathcal{H}}_i(\zeta_i,t) = [\mathbf{L}_i^T\mathbf{n}(\zeta_i)]\cdot\dot{\mathbf{F}}(t)\,, \tag{3.29b}$$
$$\frac{\partial\mathcal{H}_i}{\partial\mathbf{F}(t)} = \frac{\partial\dot{\mathcal{H}}_i}{\partial\dot{\mathbf{F}}(t)} = \mathbf{L}_i^T\mathbf{n}(\zeta_i)\,, \tag{3.29c}$$
$$T_i(\zeta_i,t) = -\frac{1}{\rho_i c_{p;i} s_i}[\mathbf{L}_i^T\mathbf{p}(\zeta_i)]\cdot\mathbf{F}(t)\,. \tag{3.29d}$$

By using (3.29d), the terms associated with the thermal potential (3.9a) provide

$$\begin{aligned}
\frac{\partial\mathcal{V}_i}{\partial\mathbf{F}(t)} &= \frac{1}{\rho_i c_{p;i} s_i}\int_0^1 [\mathbf{L}_i^T\mathbf{p}(\zeta_i)][\mathbf{L}_i^T\mathbf{p}(\zeta_i)]^T\; d\zeta_i\;\mathbf{F}(t) = \frac{1}{\rho_i c_{p;i} s_i}\mathbf{L}_i^T\mathbf{K}\mathbf{L}_i\;\mathbf{F}(t)\,,\\
\frac{\partial\mathcal{V}}{\partial\mathbf{F}(t)} &= \left[\sum_{i=1}^N \frac{1}{\rho_i c_{p;i} s_i}\mathbf{L}_i^T\mathbf{K}\mathbf{L}_i\right]\mathbf{F}(t)\,,
\end{aligned} \tag{3.30}$$

where $\mathbf{K} := \int_0^1 \left[\mathbf{p}(\zeta)\;\mathbf{p}^T(\zeta)\right]\; d\zeta$ is a 5×5 non-dimensional matrix, the same for all the N layers, whose explicit expression is recorded in the Appendix A.2.

Analogously, relations (3.29b) and (3.29c) applied to the dissipation function (3.9b) give

$$\begin{aligned}
\frac{\partial\mathcal{D}_i}{\partial\dot{\mathbf{F}}(t)} &= \frac{s_i}{\lambda_i}\int_0^1 \dot{\mathcal{H}}_i(\zeta_i,t)\;\frac{\partial\mathcal{H}_i(\zeta_i,t)}{\partial\dot{\mathbf{F}}(t)}\;d\zeta_i\\
&= \frac{s_i}{\lambda_i}\int_0^1 [\mathbf{L}_i^T\mathbf{n}(\zeta_i)][\mathbf{L}_i^T\mathbf{n}(\zeta_i)]^T\;d\zeta_i\;\dot{\mathbf{F}}(t) = \frac{1}{\rho_i c_{p;i} s_i}\mathbf{L}_i^T\mathbf{C}'\mathbf{L}_i\;\dot{\mathbf{F}}(t)\,,\\
\frac{\partial\mathcal{D}}{\partial\dot{\mathbf{F}}(t)} &= \left[\sum_{i=1}^N \frac{s_i}{\lambda_i}\;\mathbf{L}_i^T\mathbf{C}'\mathbf{L}_i\right]\dot{\mathbf{F}}(t)\,,
\end{aligned} \tag{3.31}$$

where $\mathbf{C}' := \int_0^1 \left[\mathbf{n}(\zeta)\;\mathbf{n}^T(\zeta)\right]\; d\zeta$ is a non-dimensional 5×5 matrix whose expression can also be found in Appendix A.2.

3.2.2 Boundary conditions and driving forces

The term $\mathbf{Q}$ of (3.28a) accounts for the thermal driving forces associated with the temperatures at boundaries and the interface between the layers, and can be rearranged as

$$\begin{aligned}\mathbf{Q} \quad &= \left[T_1 \frac{\partial \mathcal{H}_1}{\partial \mathbf{F}(t)}\right]_{\zeta_1=0} - \left[T_N \frac{\partial \mathcal{H}_N}{\partial \mathbf{F}(t)}\right]_{\zeta_N=1} \\ &\quad - \sum_{i=1}^{N-1} \left\{ \left[T_i \frac{\partial \mathcal{H}_i}{\partial \mathbf{F}(t)}\right]_{\zeta_i=1} - \left[T_{i+1} \frac{\partial \mathcal{H}_{i+1}}{\partial \mathbf{F}(t)}\right]_{\zeta_{i+1}=0} \right\} . \end{aligned} \tag{3.32}$$

Here, the first two terms are boundary condition of the third-kind. Following [14], they are evaluated by considering that the heat flux $\dot{\mathcal{H}}$ at the front and back boundaries $\zeta_1 = 0$ and $\zeta_N = 1$ is defined by (2.2), i.e., $\dot{\mathcal{H}}(\zeta_1, t)|_{\zeta_1=0} = q_F(t)$ and $\dot{\mathcal{H}}(\zeta_N, t)|_{\zeta_N=1} = q_B(t)$, and $\dot{\mathcal{H}}_i^*(\zeta_i, t) = E_i(\zeta_i, t)$ as per eq. (3.12). The boundary temperatures are

$$\begin{aligned} T_1(0,t) &= -\frac{1}{h_e}\left[\dot{\mathcal{H}}_1(0,t) + \dot{\mathcal{H}}_1^*(0,t)\right] + \tilde{T}_{ext}(t) \\ &= -\frac{1}{h_e}\left[\mathbf{L}_1 \mathbf{n}(0)\right] \cdot \dot{\mathbf{F}}(t) + \tilde{T}_{ext}(t)\,, \end{aligned} \tag{3.33a}$$

$$\begin{aligned} T_N(1,t) &= \frac{1}{h_i}\left[\dot{\mathcal{H}}_N(1,t) + \dot{\mathcal{H}}_N^*(1,t)\right] + T_{int}(t) \\ &= \frac{1}{h_i}\left[\mathbf{L}_N \mathbf{n}(1)\right] \cdot \dot{\mathbf{F}}(t) + \frac{\overline{\tau}_N \alpha_N G(t)}{h_i} + T_{int}(t)\,, \end{aligned} \tag{3.33b}$$

where $\tilde{T}_{ext}(t)$ is the fictitious temperature defined by (2.3). Therefore, one finds

$$\left[T_1 \frac{\partial \mathcal{H}_1}{\partial \mathbf{F}(t)}\right]_{\zeta_1=0} = -\frac{1}{h_e}\left[\ \mathbf{L}_1^T \mathbf{C}''_{ext} \mathbf{L}_1\right] \dot{\mathbf{F}}(t) + \tilde{T}_{ext}(t) \mathbf{L}_1^T \mathbf{n}(0)\,, \tag{3.34a}$$

$$\left[T_N \frac{\partial \mathcal{H}_N}{\partial \mathbf{F}(t)}\right]_{\zeta_N=1} = \frac{1}{h_i}\left[\mathbf{L}_N^T \mathbf{C}''_{int} \mathbf{L}_N\right] \dot{\mathbf{F}}(t) + T_{int}(t) \mathbf{L}_N^T \mathbf{n}(1) + \frac{\overline{\tau}_N \alpha_N G(t)}{h_i} \mathbf{L}_N^T \mathbf{n}(1)\,. \tag{3.34b}$$

The matrices $\mathbf{C}''_{int} := \mathbf{n}(1)\mathbf{n}^T(1)$ and $\mathbf{C}''_{ext} := \mathbf{n}(0)\mathbf{n}^T(0)$ are indicated in Appendix A.2.

The last term of (3.32) may be written as

$$
\begin{aligned}
&- \left\{ \left[T_i \frac{\partial \mathcal{H}_i}{\partial \mathbf{F}(t)} \right]_{\zeta_i=1} - \left[T_{i+1} \frac{\partial \mathcal{H}_{i+1}}{\partial \mathbf{F}(t)} \right]_{\zeta_{i+1}=0} \right\} \\
&= \frac{1}{\rho_i c_{p;i} s_i} \left[\left[\mathbf{L}_i^T \mathbf{p}(1) \right] \cdot \mathbf{F}(t) \right] \mathbf{L}_i^T \mathbf{n}(1) - \frac{1}{\rho_{i+1} c_{p;i+1} s_{i+1}} \left[\left[\mathbf{L}_{i+1}^T \mathbf{p}(0) \right] \cdot \mathbf{F}(t) \right] \mathbf{L}_{i+1}^T \mathbf{n}(0) \\
&= \left[\frac{1}{\rho_i c_{p;i} s_i} \mathbf{L}_i^T \mathbf{M}_1 \mathbf{L}_i - \frac{1}{\rho_{i+1} c_{p;i+1} s_{i+1}} \mathbf{L}_{i+1}^T \mathbf{M}_0 \mathbf{L}_{i+1} \right] \mathbf{F}(t) \,. \qquad (3.35)
\end{aligned}
$$

The expressions for the matrices $\mathbf{M}_1 = \mathbf{n}(1)\mathbf{p}^T(1)$ and $\mathbf{M}_0 = \mathbf{n}(0)\mathbf{p}^T(0)$ can be found in Appendix A.2. Observe, in passing, that since the temperature field in the layered pane is continuous as per (3.23), these terms are due to the discontinuities of the heat displacement at the interfaces.

By defining the non-dimensional interface matrix

$$
\mathbf{M}_{i;i+1} = \mathbf{L}_i^T \mathbf{M}_1 \mathbf{L}_i - \frac{1}{\beta_{i;i+1}} \mathbf{L}_{i+1}^T \mathbf{M}_0 \mathbf{L}_{i+1} \,, \qquad (3.36)
$$

with $\beta_{i;i+1}$ given by (3.24), the expression (3.32) for $\mathbf{Q}$ can be written as

$$
\begin{aligned}
\mathbf{Q} \quad &= - \left[\frac{1}{h_e} \left[\, \mathbf{L}_1^T \mathbf{C}''_{ext} \mathbf{L}_1 \right] + \frac{1}{h_i} \left[\mathbf{L}_N^T \mathbf{C}''_{int} \mathbf{L}_N \right] \right] \dot{\mathbf{F}}(t) \\
&\quad + \left[\sum_{i=1}^{N-1} \frac{1}{\rho_i c_{p;i} s_i} \mathbf{M}_{i;i+1} \right] \mathbf{F}(t) + \tilde{\mathbf{b}}(t) + \mathbf{b}^+(t) \,, \qquad (3.37)
\end{aligned}
$$

where $\tilde{\mathbf{b}}(t) = \tilde{T}_{ext}(t) \mathbf{L}_1^T \mathbf{n}(0) - T_{int}(t) \mathbf{L}_N^T \mathbf{n}(1)$ represents the forcing terms due to the heat exchange with the surrounding environment, while $\mathbf{b}^+(t) := -\frac{\overline{\tau}_N \alpha_N G(t)}{h_i} \mathbf{L}_N^T \mathbf{n}(1)$ is an additional driving force, related to the variation of heat flux along the panel thickness due to the distributed effect of the solar radiation. Notice that the time-dependence is due to the variation of the environmental conditions.

For what concerns the term $\mathbf{Q}^*$ (3.28b), accounting for the absorption of the solar radiation, this can be readily evaluated as

$$
\mathbf{Q}^* = - \sum_{i=1}^{N} \frac{s_i}{\lambda_i} \int_0^1 E_i(\zeta_i, t) \; \mathbf{L}_i^T \mathbf{n}(\zeta) \; d\zeta =: \mathbf{b}^*(t) \,. \qquad (3.38)
$$

When approximation (2.7) is used for the absorbed energy $E_i(\zeta_i, t)$,

$$\mathbf{b}^*(t) = -\sum_{i=1}^{N} \frac{s_i}{\lambda_i}\, \overline{\tau}_i \alpha_i\, G(t)\, \mathbf{L}_i^T \mathbf{a}\,, \tag{3.39}$$

where $\mathbf{a} := \int_0^1 \zeta \mathbf{n}(\zeta)\, d\zeta$ is detailed in Appendix A.2.

3.2.3 Matrix form of the discretized problem

From (3.30), (3.31), (3.37) and (3.39), the variational principle provides the linear system of differential equations

$$\mathbf{K}_{tot}\, \mathbf{F}(t) + \mathbf{C}_{tot}\, \dot{\mathbf{F}}(t) = \mathbf{b}(t)\,, \tag{3.40}$$

where

$$\mathbf{K}_{tot} := \sum_{i=1}^{N} \frac{1}{\rho_i c_{p;i} s_i} \mathbf{L}_i^T \mathbf{K} \mathbf{L}_i - \sum_{i=1}^{N-1} \frac{1}{\rho_i c_{p;i} s_i} \mathbf{M}_{i;i+1}\,, \tag{3.41a}$$

$$\mathbf{C}_{tot} := \sum_{i=1}^{N} \frac{s_i}{\lambda_i}\, \mathbf{L}_i^T \mathbf{C}' \mathbf{L}_i + \frac{1}{h_e} \left[\, \mathbf{L}_1^T \mathbf{C}''_{ext} \mathbf{L}_1 \right] + \frac{1}{h_i} \left[\mathbf{L}_N^T \mathbf{C}''_{int} \mathbf{L}_N \right]\,, \tag{3.41b}$$

$$\mathbf{b}(t) := \tilde{\mathbf{b}}(t) + \mathbf{b}^+(t) + \mathbf{b}^*(t)\,. \tag{3.41c}$$

In the language of structural dynamics, $\mathbf{K}_{tot}$ plays the role of the stiffness matrix, and now accounts for the temperature distribution in the layers and for the discontinuities of the heat displacement fields at their interfaces. Analogously, $\mathbf{C}_{tot}$ is the counterpart of the damping matrix [52, 20], which considers the bulk dissipation and the dissipation from the heat transfer at the boundary. The vector $\mathbf{b}(t)$ is the analogue of the externally applied forces, which are now the thermal driving forces. In general $\mathbf{K}_{tot}$ and $\mathbf{C}_{tot}$ are band matrices.

It is useful to re-write (3.40) in terms of the sub-vectors defined in (3.25), in the form

$$[\mathbf{K}_{tot;T} | \mathbf{K}_{tot;H}] \begin{bmatrix} \mathbf{F}_T(t) \\ \hline \mathbf{F}_H(t) \end{bmatrix} + [\mathbf{C}_{tot;T} | \mathbf{C}_{tot;H}] \begin{bmatrix} \dot{\mathbf{F}}_T(t) \\ \hline \dot{\mathbf{F}}_H(t) \end{bmatrix} = \mathbf{b}(t)\,, \tag{3.42}$$

where $\mathbf{K}_{tot;T}$ and $\mathbf{C}_{tot;T}$ are $(3N+2) \times (2N+2)$ matrices, while $\mathbf{K}_{tot;H}$ and $\mathbf{C}_{tot;H}$ are $(3N+2) \times N$ matrices.

It can be verified that, due to the choice of the generalized coordinates, $\mathbf{K}_{tot;H} = \mathbf{0}$. Therefore, $\mathbf{F}_H(t)$ cannot be determined by solving the system (3.42), which provides only its

time derivative $\dot{\mathbf{F}}_H(t)$. The values of $\mathbf{F}_H(t)$ will depend on the initial conditions prescribed on the heat displacement but, as already discussed in Section 3.1, these remain arbitrary according to the definition of $\mathcal{H}$.

The system (3.42) can be easily solved. A particular case is that in which the boundary conditions are constant in time, that is $\mathbf{b}(t) = \mathbf{b}$. The corresponding asymptotic *steady state* solution can be found by requiring that $\partial T_i(\zeta_i, t)/\partial t = 0 \ \forall \ i = 1, \ldots, N$: recalling (3.21) and (3.25), this implies $\mathbf{F}_T(t) = const\,,\ \dot{\mathbf{F}}_T(t) = 0$. Observe that the associated temperature distribution corresponds to a heat flux $\dot{\mathcal{H}}_i$ constant in time and uniform along the element thickness, for which $\dot{\mathbf{F}}_H(t) = const$.

The steady state hence corresponds to the solution of

$$[\mathbf{K}_{tot;T}|\ \mathbf{0}\ ] \left[\frac{\mathbf{F}_T}{\mathbf{F}_H(t)}\right] + [\mathbf{C}_{tot;T}|\mathbf{C}_{tot;H}] \left[\frac{\mathbf{0}}{\dot{\mathbf{F}}_H}\right] = [\mathbf{K}_{tot;T}|\mathbf{C}_{tot;H}] \left[\frac{\mathbf{F}_T}{\dot{\mathbf{F}}_H}\right] = \mathbf{b}\,, \quad (3.43)$$

which is a system of $(3N + 2)$ *algebraic* equations, from which one finds the $(2N + 2)$ components of $\mathbf{F}_T$ and the N components of $\dot{\mathbf{F}}_H$.

3.3 Advantages with respect to standard FEM approaches

The standard FEM approach [61, 35] starts from the governing equation (2.8) for the i-th layer. The steady-state problem is formulated in the weak form, by multiplying the governing equation and the boundary conditions by an arbitrary weight function. For one layer ($N = 1$), denoting by $v(\zeta)$ the weight function, one obtains

$$\int_0^1 \left[\frac{\lambda}{s^2}\frac{\partial^2 T(\zeta)}{\partial \zeta^2} + \frac{1}{s}\frac{\partial E(\zeta)}{\partial \zeta}\right]\ v(\zeta)\ d\zeta + \text{boundary terms} = 0\,. \quad (3.44)$$

where the detailed expression of the boundary terms can be found, e.g., in [61, 35].

Then, both the temperature field and the weight function are approximated by using spatial shape functions[4], in a form analogous to (3.21b), determined by the nodal values. The most used shape functions are of the first order. In general, this choice does not satisfy the differential equation and boundary conditions: this results in an error called *residual*, estimated by substituting the approximated solution $\tilde{T}(\zeta)$ into the governing differential expression, i.e.,

[4] In the most used approach *à la* Galerkin, the same shape functions for the temperature field are used for the weight functions.

$$r(\tilde{T}(\zeta)) := \frac{\lambda}{s^2}\frac{\partial^2 \tilde{T}(\zeta)}{\partial \zeta^2} + \frac{1}{s}\frac{\partial E(\zeta)}{\partial \zeta} + \text{boundary terms}\,. \tag{3.45}$$

The weak formulation (3.44) provides a system of algebraic equations for the nodal values, which corresponds to the zeroing of the weighted average of the residuals. Hence, it is usually referred to as the Weighted Residual Method. Since the shape functions are usually chosen so to satisfy the boundary conditions, as well as continuity interface conditions, the obtained solution is accurate at these points: the accuracy in the interior is obtained by dividing the thickness in finite elements.

For transient problems, the time dependence of the temperature field is usually considered via a finite difference approximation [61, 19]. The solution at the first time step is obtained by solving a set of algebraic equations; at each subsequent time step, the solution is evaluated by considering a modified force vector, accounting for the forcing terms at boundaries, and by using coefficient matrices dependent on the size of the time increment. The accuracy depends the size of both the spatial mesh and the time step [39, 57, 11]. For the thermal problems of architectural glazings, simpler methods are often used, consisting in discretizing the governing equation of the problem by means of finite difference techniques, in both space and time [36, 9, 10].

In all the aforementioned approaches, the condition of energy conservation is only approximately satisfied. To this respect, the proposed method based on Biot's variational approach is more consistent, because energy conservation is equivalent to an holonomic constraint, not involving time, as per (3.1), which is rigorously verified at each time. This improves the quality of the solution, especially for what concerns the relation between temperature field and heat flux.

In addition, it should be mentioned that traditional continuous Galerkin FEMs are not efficient in evaluating the peak values of temperatures and heat flux in thermal problems involving high temperature gradients, even when a very refined mesh is used. For this kind of problems, refined finite element formulations have been developed to efficiently capture steep gradients. For example, the generalized finite element method represents a direct extension of the standard FE method, enabling the accurate approximation of solutions with jumps, kinks, singularities, and other locally non-smooth features within elements [55, 29, 47]. The discontinuous Galerkin FEM [21, 41], first introduced by Reed and Hill [50] for the analysis of neutron transport problems, allows for discontinuities of the physical unknowns within the interior of the problem domain. The coordinate transformation approaches are capable of conforming to the nonuniform and steep temperature profiles [8, 37]. However, the difficulty is bypassed when using Biot's variational principle, because in (3.16) the spatial derivatives of $T_i(\zeta_i, t)$ are not involved. This is a direct consequence of the fact that the basic unknown field, to be determined, is not the temperature field, but the heat displacement field, which is related to the spatial integral of $T_i(\zeta_i, t)$, as per (3.8).

Moreover, the standard FEM approach does not permit the heat flux to be directly

evaluated. It must be recovered *a posteriori* once the (approximate) temperature field is known. On the other hand, the fields for the temperature, the heat displacement and the heat flux can be directly evaluated in Biot's variational approach, by using (3.29a), (3.29b), (3.29d).

In particular, the proposed method presents a great advantage for what concerns the evaluation of the thermal stress. Indeed, the traditional FEM methods, based on linear shape functions, provide an approximated piecewise linear temperature distribution that, as discussed in Section 2.3, may provide an erroneous estimate of the thermal stress because the incompatibility of the thermal strain is concentrated at those points where the temperature profile is not smooth. Moreover, the use of shape function of order higher than one does not require a fine discretization, since the nodal points can be made to correspond to the boundary of each layer, i.e., only one finite element per layer is required.

4 Examples and comparisons

To illustrate the FEM approach based on the Biot's variational method, hereafter referred to as BVM, the worked examples are those of a monolithic glass plate and a laminated glass pane composed of two glass plies bonded by a PVB interlayer. Table 1 summarizes the assumed physical and thermal properties of the materials.

Table 1: Values of physical and thermal properties of materials considered in the proposed examples.

Material	Reference	ρ [kg/m^3]	c_p [J/(kg K)]	λ [W/(m K)]	α [−]	τ [−]	ε [−]
glass	[7, 2]	2500	720	1	0.23	0.67	0.837
PVB	[9, 18]	1087	1360	0.236	0.01	0.99	0

The values of the convective heat transfer coefficients h_{eC} =8 W/(m^{2}K) and h_{iC} = 3.6 W/(m^{2}K), are taken from EN ISO 6946 [4] and EN 410 [5], respectively. Since the glass surface temperatures are unknown, the radiant coefficients h_{iR} and h_{eR} are evaluated according to (2.1), by conventionally assuming the glass temperature equal to 10 °C.

We first consider *fixed external conditions* for a standard values winter scenario [3, 30], for which G = 800 W/m^2, T_{ext} = −12°C, T_{sky} = −5°C, T_{int} = 25 °C. Successively, we analyze *daily variation* of environmental parameters as in [30]. In both cases, the solar radiation is modeled by considering a linear attenuation according to (2.7).

The obtained results are compared with a direct numerical solution of the heat-conduction partial differential equation under the aforementioned boundary and initial conditions. This is done with the "pdepe" Matlab tool [45], conceived for solving parabolic and elliptic partial differential equations of one spatial variable and time. Since a discretization in both

space and time is required, the direct solution is found computationally more expensive than the proposed BVM.

4.1 Transient state for fixed environmental conditions

The transient solution is calculated under fixed external temperatures T_{ext} and T_{sky}, and solar radiation G. In the BVM, the temperature field is calculated by solving the system (3.40).

As initial condition, it is required that, at $t = 0$, the front temperature $T_1(\zeta_1, 0)|_{\zeta_1=0}$ is equal to the fictitious temperature $\tilde{T}_{ext}$, accounting both for the convective and radiative heat exchange with the external environment, while the back temperature $T_N(\zeta_N, 0)|_{\zeta_N=1}$ equals the inner temperature T_{int}. The temperature profile at $t = 0$ is assumed to be piecewise linear and respecting the continuity conditions (2.10). Furthermore, at $t = 0$, the part of the heat displacement related to the temperature field is null at the back surface, and continuous at the interfaces[5], i.e., $\mathcal{H}_N(\zeta_N, 0)|_{\zeta_N=1} = 0$ and $\mathcal{H}_i(\zeta_i, 0)|_{\zeta_i=1} = \mathcal{H}_{i+1}(\zeta_i, 0)|_{\zeta_{i+1}=0}$.

4.1.1 Monolithic glass

Consider a 12 mm thick monolithic glass panel. The generalized coordinates $f_{1,k}(t)\,,\ k = 1, \dots, 5$, evaluated by solving (3.40), are plotted in Figure 2 as a function of time. Observe that $f_{1,k}(t)\,,\ k = 1, \dots, 4$, tend to become constant after a certain time of the order of one hour: in agreement with [30], no heat is stored and temperature becomes constant. Notice as well that $f_{1,1}(t)$ and $f_{1,2}(t)$, respectively associated with the temperatures at the front and back surfaces, exhibit a very similar trend. On the other hand, the coordinate $f_{1,5}(t)$ which, as discussed in Sect. 3.3, does not influence the temperature field, tends to linearly increase in time. This corresponds to a constant heat flux $\dot{\mathcal{H}}$.

Once the vector of the generalized coordinates $\mathbf{F}(t)$ is known, the temperature field $T_1(\zeta_1, t)$ and the heat flux $\dot{\mathcal{H}}_1(\zeta_1, t)$ are evaluated according to (3.29d) and (3.29b), respectively. Figure 3(a) shows the front and back temperatures $T_F(t) = T_1(0, t)$ and $T_B(t) = T_1(1, t)$ and the corresponding steady-state values. These are evaluated either with the BVM, by solving the algebraic system (3.43), or by numerically solving the heat equation (2.8) with boundary conditions (2.9). To emphasize the spatial dependence of $T_1(\zeta_i, t)$, Figure 3(b) shows the temperature profile at different times. The numerical solution is also plotted in the same graphs with blue lines, but it cannot be distinguished because it perfectly overlaps with the BVM results.

It is confirmed that the front and back temperatures converge to the steady-state values

[5]It has been verified that very similar results may be obtained by considering, instead, null heat displacement at the front surface. Indeed, the boundary condition prescribed on the heat displacement affects neither the temperature field nor the heat flux.

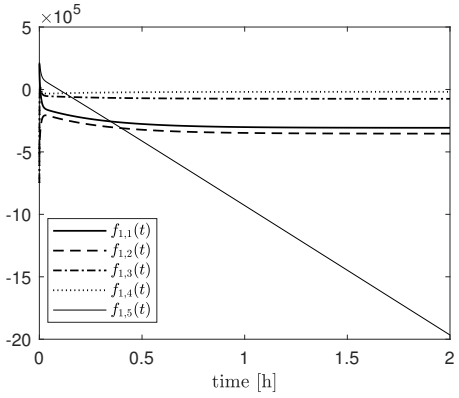

Figure 2: Monolithic glass under fixed environmental conditions. Generalized coordinates $f_{1,k}(t)$, $k = 1, \ldots, 5$ as a function of time.

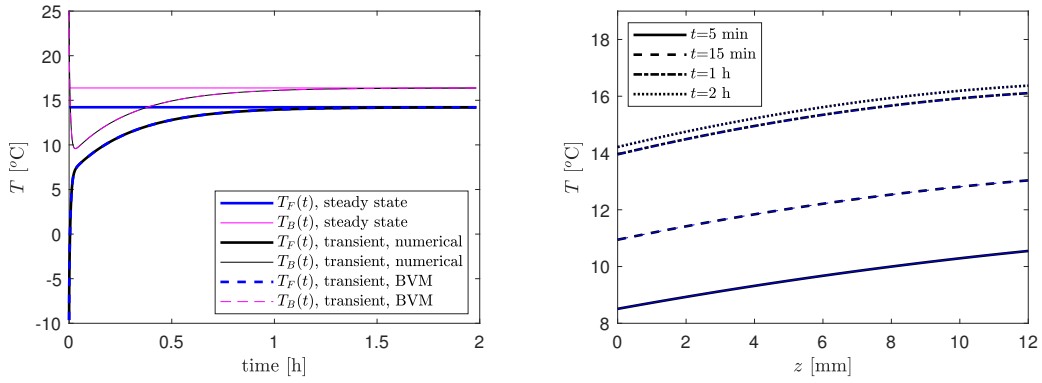

Figure 3: Monolithic glass under fixed environmental conditions. a) Comparison between front and back temperatures $T_F(t)$ and $T_B(t)$ and the steady-state solution; b) temperature profile in the glass thickness at different times t. Direct numerical results are also plotted for comparison.

in about 1 hour. There is perfect agreement between the BVM results and the direct numerical solution, being the maximum error[6] of the order of 0.07°C for $t > 10$ s.

The *total* heat flux $\dot{\overline{\mathcal{H}}}_1(\zeta_1, t) = \dot{\mathcal{H}}_1(\zeta_1, t) + \dot{\mathcal{H}}_1^*(\zeta_1, t)$ may be evaluated according to equation (3.11), where $\dot{\mathcal{H}}_1(\zeta_1, t)$ comes from (3.29b). Figure 4(a) shows the values in correspondence of the front and back surfaces, i.e., $\dot{\overline{\mathcal{H}}}_F(t) = \dot{\overline{\mathcal{H}}}_1(0, t)$ and $\dot{\overline{\mathcal{H}}}_B(t) = \dot{\overline{\mathcal{H}}}_1(1, t)$: these account for the heat from solar radiation absorbed in the glass thickness. The in-the-thickness profile at different times is represented in Figure 4(b). No comparisons are made with the solution found with the numerical procedure, because this directly determines only the temperature field.

From Figure 4(a), it is evident that, after approximatively 1 hour, the front and back

[6]For t <10 s, a maximum error of about 0.8°C is found for very low values of t.

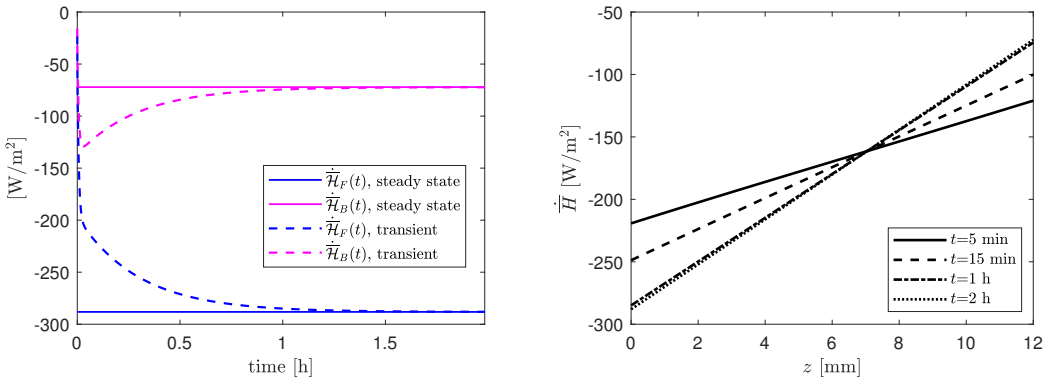

Figure 4: Monolithic glass under fixed environmental conditions. a) Comparison between front and back heat fluxes $\dot{\mathcal{H}}_F(t)$ and $\dot{\mathcal{H}}_B(t)$ and the steady-state solution; b) in-the-thickness heat flux profiles at various times.

heat fluxes tend to the steady state condition. The difference between the two values obviously corresponds to the heat absorbed in the glass thickness[7]. Notice than both the heat fluxes are negative: in the winter scenario, heat flows from the internal environment to glass, and then to the external environment.

4.1.2 Laminated glass

Consider a laminated pane with two glass plies of thickness $s_1 = 8$ mm and $s_3 = 6$ mm, bonded by a PVB interlayer of thickness $s_2 = 1.52$ mm. In the system (3.40) now $N = 3$.

Figure 5(a) reports the variation in time of the front and back temperatures and of the interface temperatures $T_{int1,2}(t) := T_1(1,t) = T_2(0,t)$ and $T_{int2,3}(t) := T_2(1,t) = T_3(0,t)$, with evidence of the asymptotic steady state obtained by solving (3.43). The results numerically obtained, also shown, cannot be distinguished because they perfectly overlap with the BVM solution. Observe that now the time required for the steady-state is of the order of 1.5 hours, being slightly higher for the back temperatures due to the heat storage in the laminated pane.

Figure 5(b) shows the temperature profile at various times. Again the curves obtained by numerically solving the equation are not plotted because they perfectly overlap, being the maximum difference[8] of the order of 0.02°C for t >10 s. As expected, at the interfaces

[7]Notice that, since the solar radiation is considered to be absorbed along the glass thickness, no energy is absorbed at $\zeta_1 = 0$, and hence $\dot{\mathcal{H}}_F(t)$ does not account for this contribution. At the steady state condition, the energy balance requires that the sum of energies incoming in the panel (convective/radiant fluxes from the external environment and solar radiation) is equal to the energy releases by the panel to the internal environment. Hence, the back flux $\dot{\mathcal{H}}_B(t)$ is affected by the solar radiation.

[8]For t <10 s, the maximum difference is 0.36°C, occurring at the very beginning.

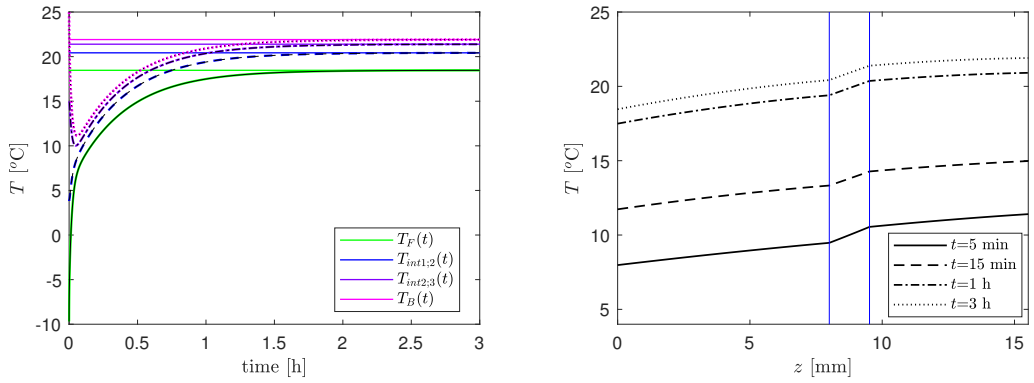

Figure 5: Laminated glass under fixed environmental conditions. a) Histories of front, back and interface temperatures and steady-state; b) temperature profile in the pane thickness at different times. Direct numerical results are also shown for comparison.

the slope of the temperature curves respect $(2.10)_2$. For high values of t, the temperature profile tends to be piecewise parabolic.

Figure 6(a) shows the front and back heat fluxes, as well as the heat fluxes at the glass-polymer interfaces $\dot{\overline{\mathcal{H}}}_{int1,2}(t) = \dot{\overline{\mathcal{H}}}_1(1,t) = \dot{\overline{\mathcal{H}}}_2(0,t)$ and $\dot{\overline{\mathcal{H}}}_{int2,3}(t) := \dot{\overline{\mathcal{H}}}_2(1,t) = \dot{\overline{\mathcal{H}}}_3(0,t)$. As for monolithic glass, the heat fluxes are lower than zero, corresponding to heat flowing from the internal environment, to the pane, and then to the external environment. Observe that, in the steady state, the heat flux is monotonically increasing along the laminated glass element.

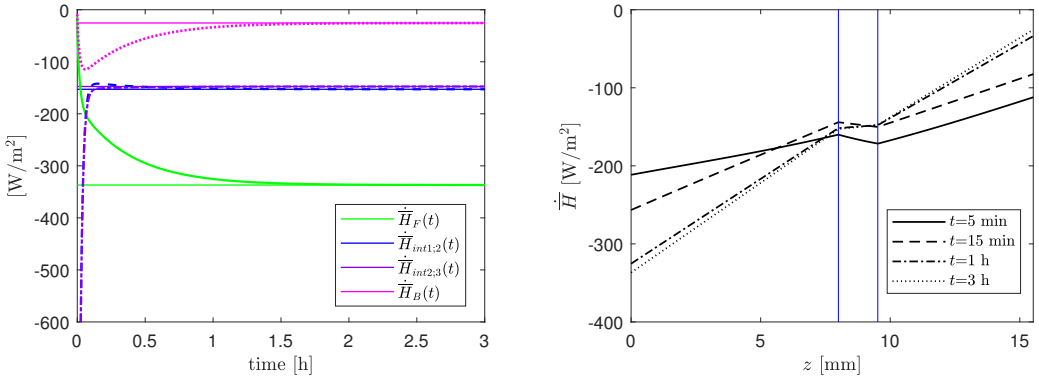

Figure 6: Laminated glass under fixed environmental conditions. a) Front, back and interface heat fluxes as a function of time and steady-state solution; b) in-the-thickness heat flux profile at various times.

4.2 Transient state under variable environmental conditions

The solar radiation $G(t)$ and the external temperature $T_{ext}(t)$ are now made to vary according to daily variations. Following [30], the time dependence of $G(t)$ is approximated with a parabolic law, while $T_{ext}(t)$ is assumed sinusoidal in time. Approximately, $T_{sky}(t)$ is set equal to $T_{ext}(t)$, and we use the same values of h_{eR} and h_{iR} considered in Section 4.1. The time dependent temperature field is evaluated by solving (3.40). Since the solution shall be periodic in time (temperature and heat flux at $t = 0$ shall equal those at $t = 24$ h), an iterative procedure has been used[9] until $\mathbf{F}_T(0) = \mathbf{F}_T(24\text{ h})$ and $\dot{\mathbf{F}}_H(0) = \dot{\mathbf{F}}_H(24\text{ h})$.

Again, the results from the BVM are compared with the direct numerical solution of the equations via the "pdepe" Matlab tool [45]. An iterative procedure has been used to achieve that the front, back and interface temperatures at $t = 0$ are equal to those at $t = 24$ h. It has to be mentioned that, when time-dependent boundary conditions are used, the direct numerical solution is strongly sensitive to the time and spatial mesh[10].

4.2.1 Monolithic glass

Consider, first, the monolithic glass pane already analyzed in Section 4.1.1, for which the relevant equations are (3.40), with $N = 1$. The nodal values $f_{1,k}(t)\,,\ k = 1, \dots, 4$ are plotted in Figure 7, for the considered winter scenario. Obviously, the values do not tend to zero as $t \to \infty$: since the external conditions change in time, a steady state cannot be reached.

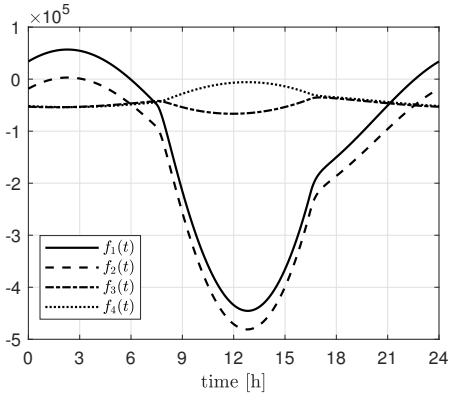

Figure 7: Monolithic glass under variable environmental conditions. Nodal values $f_{1,k}(t)\,,\ k = 1, \dots, 4$ as a function of time.

The graphs in Figure 8(a) show the time-dependent front and back temperatures evaluated with the proposed approach and their comparison with the direct numerical solution.

[9] In the worked examples, the rate of convergence is very high, since the solution is obtained with two iterations.

[10] Results shown in Figures 8(a) and 8(b) have been obtained by dividing the glass thickness in 100 elements.

Figure 8(b) indicates the in-the-thickness temperature profiles at various times of the day. The temperatures obviously follow the variation of environmental condition, with a small delay due to heat storage[11]. There is a very good agreement between the proposed method and numerical solution (maximum error of the order of 0.4°C). The proposed method is computationally much more efficient than the direct numerical solution, which requires a fine discretization in both space and time.

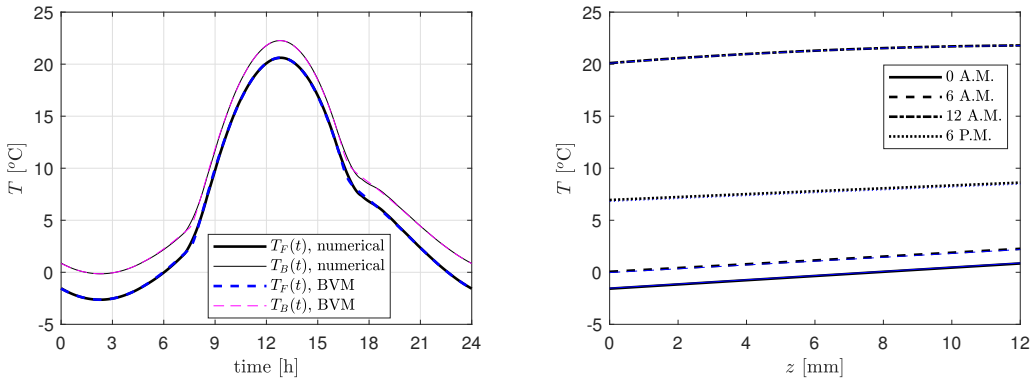

Figure 8: Monolithic glass under environmental conditions. a) Time history of front and back temperatures $T_F(t)$ and $T_B(t)$ and b) temperature distribution along the glass thickness at various hours of the day.

Figure 9(a) reports, as a function of time, the values of the total heat flux at the front and back surfaces, accounting for the heat absorbed along the glass thickness. Figure 9(b) shows the in-the-thickness heat flux profiles at various hours of the day. Observe that the heat fluxes are now strongly dependent upon the environmental conditions. In particular, during the night hours, when the solar radiation is null[12], $\dot{\overline{\mathcal{H}}}_B(t)$ presents a small delay (of less than 1 hour) with respect to the front heat flux $\dot{\overline{\mathcal{H}}}_F(t)$, due to the heat storage in the element thickness. During the central hours of the day, there is instead a strong difference between the two values, due to the solar radiation absorbed by the glass that is now variable along the day.

4.2.2 Laminated glass

For the laminated glass pane already considered in Section 4.1.2, but now under variable environmental conditions, Figure 10(a) shows the time variation of the front and back temperatures $T_F(t)$ and $T_B(t)$, as well as of interface temperatures $T_{int1,2}(t)$ and $T_{int2,3}(t)$. Again, the results from the direct numerical solution are plotted for the sake of comparison. The trend is similar to that of Figure 8(a) for monolithic glass, but it is evident that there is a temperature decrease when passing from the external surface to the glass-polymer

[11] According to [31], this delay is expected to be higher for insulated glass units.
[12] In the winter scenario the solar radiation is nil [30] from 4.30 P.M. to 7.30 A.M.

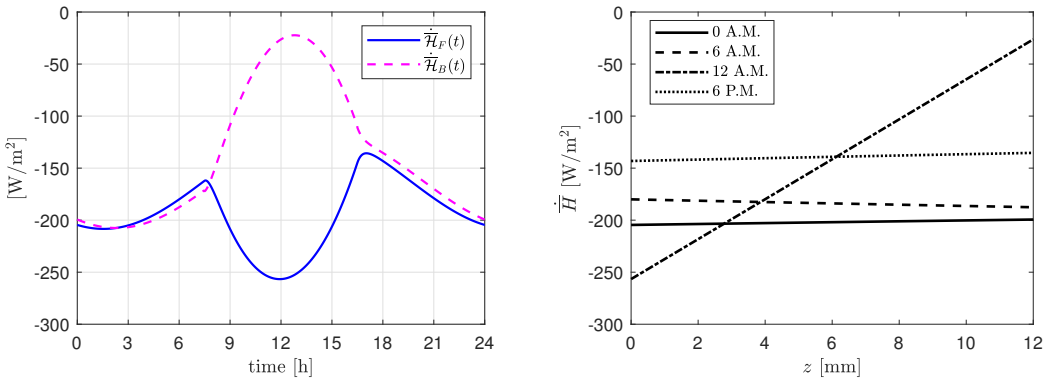

Figure 9: Monolithic glass under variable environmental conditions. a) Time evolution of the front and back heat fluxes $\dot{\mathcal{H}}_F(t)$ and $\dot{\mathcal{H}}_B(t)$, and b) in-the-thickness heat flux profile at various hours of the day.

interfaces, and to the back surface. This is more evident during the night hours, when the difference between external and internal temperature is higher. The differences between the results from the proposed method and the direct numerical integrations are lower than 0.02 °C. Figure 10(b) shows the in-the-thickness temperature profiles, at different hours of the day. In this case, one can drive similar conclusions to those indicated under fixed environmental conditions.

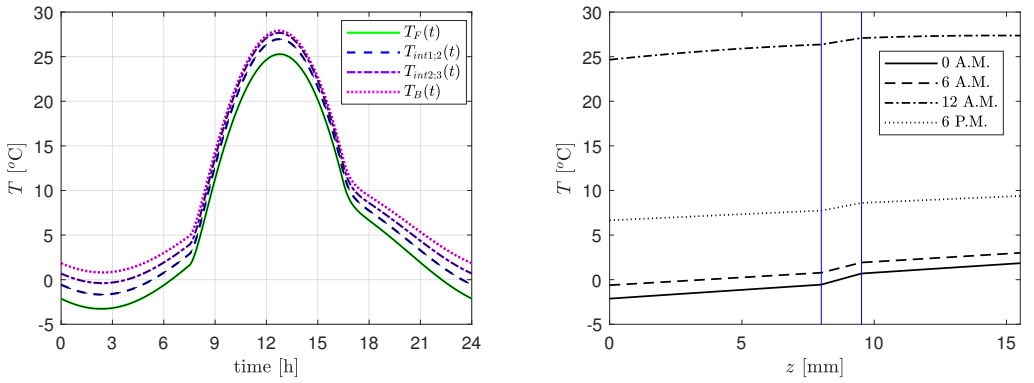

Figure 10: Laminated glass under variable environmental conditions. a) Front, interface and back temperatures (comparisons between the proposed method and direct numerical results), and b) in-the-thickness temperature profile at various hours of the day.

The heat fluxes evaluated with the BVM are plotted, as a function of time, in Figure 11(a). Here we report the front and back heat fluxes $\dot{\mathcal{H}}_F(t)$ and $\dot{\mathcal{H}}_B(t)$, as well as the interface fluxes $\dot{\mathcal{H}}_{int1,2}(t)$ and $\dot{\mathcal{H}}_{int2,3}(t)$, defined as in Section 4.1.2. Figure 11(b) shows the in-the-thickness profile at various hours of the day.

Again, the discrepancy between the front and the back flux is related to the solar radia-

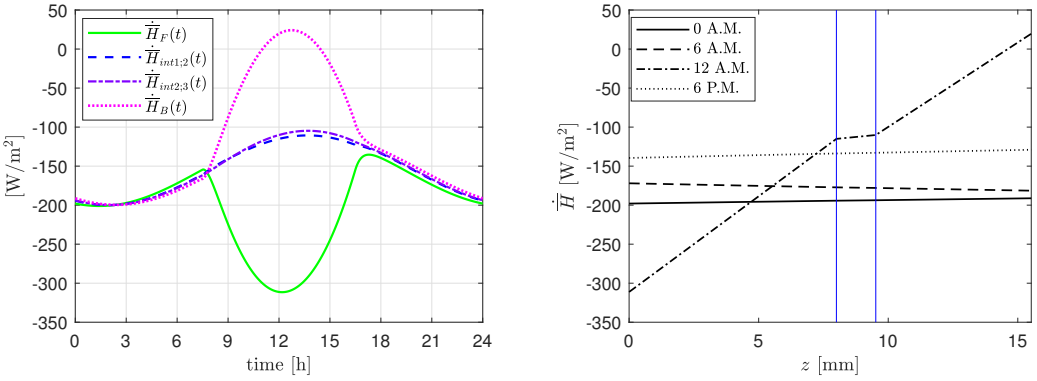

Figure 11: Laminated glass under variable environmental conditions. a) Front, interface and back heat fluxes, and b) in-the-thickness heat flux profile at various hours of the day.

tion absorbed across the laminated glass thickness and, consequently, it is more evident in the central hours of the day. Since the polymeric interlayer presents a very low absorptivity as per Table 1, the interface heat fluxes $\dot{\mathcal{H}}_{int1,2}(t)$ and $\dot{\mathcal{H}}_{int2,3}(t)$ are almost unaffected by $G(t)$, whereas they are significantly influenced by the time variation of the environmental temperature. Observe, again, that the interface heat fluxes and, even more so, the back flux, present a time delay with respect to the front flux, due to the heat storage in the different glass plies of the laminate.

5 Conclusions

The ingenious variational approach proposed by Biot in the fifties has been here used to evaluate the temperature and heat flux distribution in a layered glazing, with specific reference to laminated glass panes composed of an arbitrary number of plies with different physical and thermal properties. This weak formulation of the heat-conduction problem permits a FEM formulation to be developed, where the relevant fields are approximated with Hermite shape functions of high order, in order to allows a precise assessment the consequent thermal stress. The proposed approach allows for a direct evaluation not only of the temperature distribution, but also of the heat flux. The worked examples illustrate the temperature distribution in case of either fixed or variable environmental conditions. The results are in perfect agreement with those obtained by a direct numerical solution of the governing partial differential equation, which however is much more time-consuming because it requires a fine discretization in both space and time. In case of fixed external conditions, the time required to reach the steady state in monolithic glass is of the order of one hour, but it increases for laminated glass. Since in such a period of time the environmental conditions can substantially vary, it is in general necessary to consider the transient state in a changing environment. Consideration of heat storage in the glass, which is often neglected

in the practice, implies that the in-the-thickness temperature profile is not piecewise liner: this is very important for the determination of the thermal stress. The evaluation in time of the heat fluxes highlights that the heat storage in the different layers leads to a delay in the response, when passing from the front to the back surface.

The use of Biot's Variational Method (BVM) presents advantages with respect to other, more traditional, numerical formulations, usually based on Galerkin weighted residual FEM method for space and on finite difference discretization in time. In particular, the BVM exactly considers energy conservation in the form of a holonomic constraint (not involving time). Furthermore, since it does not involve the temperature gradient, it appears to be more efficient for thermal problems with steep temperature variations, since there is no need of a refined mesh. Finally, the BVM is very appropriate when one is particularly interested in determining the thermally-induced stress, as in the structural design of glass. In fact, the traditional FEM methods usually implement a piecewise-linear temperature profile, which provides a spurious evaluation of the thermal stress in a neighborhood of those points where the profile is not smooth. The higher-order shape functions used in the BVM approach bypass this problems and render the evaluated thermal stresses more realistic.

The implemented problem is 1-D at this stage, but the same procedures here illustrated could be extended to cover the 3-D case. This development is necessary because in architectural glazing the solar radiation is typically uneven due to the presence of shadows (from sunshades, fins, parts of adjacent buildings, contouring frame), and the heating in the internal environment can be irregular, especially when HVAC systems are present. Therefore, any accurate evaluation of the time-dependent temperature field in the glass panes requires three-dimensional modeling, which considers the different heat exchange phenomena in the in-plane direction, where the thermal problem is governed by the heat conduction between differently irradiated regions, and in through-the-thickness direction, where the effects of penetrating solar radiation and heat exchange with the surrounding environment are dominant. Although the 1D implementation only considers the effects in the thickness, it has been useful in demonstrating the advantages of an approach based on Biot's variational principle.

Acknowledgements. This research was internally supported by Maffeis Engineering SpA, Solagna (Vi), Italy, in collaboration with the University of Parma, Italy.

References

[1] ISO15099 – Thermal Performance of windows, doors and shading devices – Detailed calculation. Standard, ISO/TC 163/SC 2, 2003.

[2] N180E – Glass and Thermal Safety. Standard, CEN/TC129/WG8 – Pilkington, 2004.

[3] NF DTU 39 P3 Travaux de bâtiment – Travaux de vitrerie-miroiterie – Partie 3: Mémento calculs des contraintes thermiques. Standard, CSTB, 2006.

[4] EN ISO 6946 – Building components and building elements – Thermal resistance and thermal transmittance – Calculation method. Standard, ISO/TC 163 and CEN/TC 89, 2007.

[5] EN 410 – Glass in building – Determination of luminous and solar characteristics of glazing. Standard, CEN/TC 129, 2011.

[6] EN 673 – Glass in building – Determination of thermal transmittance (U value) – Calculation method. Standard, CEN/TC 129, 2011.

[7] EN 572-1 – Glass in building – Basic soda lime silicate glass products. Part 1: Definitions and general physical and mechanical properties. Standard, CEN/TC 129, 2012.

[8] Mark Ainsworth and Bill Senior. Aspects of an adaptive hp-finite element method: Adaptive strategy, conforming approximation and efficient solvers. *Computer Methods in Applied Mechanics and Engineering*, 150(1-4):65–87, 1997.

[9] G Alvarez, J J Flores, and C A Estrada. The thermal response of laminated glass with solar control coating. *J Phys D: Appl Phys*, 31(21):3057, 1998.

[10] G Alvarez, D N Jimenez, and C A Estrada. Thermal performance of solar control coatings: a mathematical model and its experimental verification. *J Phys D: Appl Phys*, 31(18):2249, 1998.

[11] A K Aziz and J-L Liu. A Galerkin method for the forward-backward heat equation. *Math Comput*, 56(193):35–44, 1991.

[12] C Bedon, X Zhang, F Santos, D Honfi, M Kozłowski, M Arrigoni, L Figuli, and D Lange. Performance of structural glass facades under extreme loads–Design methods, existing research, current issues and trends. *Construct Build Mater*, 163:921–937, 2018.

[13] M A Biot. New methods in heat flow analysis with application to flight structures. *J Aeronaut Sci*, 24(12):857–873, 1957.

[14] M A Biot. *Variational principles in heat transfer. A unified Lagrangian analysis of dissipative phenomena*. Oxford University Press, London, 1970.

[15] M A Biot. New variational-Lagrangian irreversible thermodynamics with application to viscous flow, reaction–diffusion, and solid mechanics. *Adv Appl Mech*, 24:1–91, 1984.

[16] A Bonati, G Pisano, and G Royer Carfagni. Redundancy and robustness of brittle laminated plates. overlooked aspects in structural glass. *Compos Struct*, 227:111288, 2019.

[17] D E Carlson. Linear thermoelasticity. In C Truesdell, editor, *MECHANICS OF SOLIDS II - Linear theories of elasticity and thermoelasticity: Linear and nonlinear theories of rods, plates, and shells*. Springer, 1984.

[18] C Carrot, A Bendaoud, C Pillon, O Olabisi, and K Adewale. Polyvinyl butyral. In *Handbook of Thermoplastics, red.*, pages 89–138. ACRC Press, 2016.

[19] J P Carter and J R Booker. Finite element analysis of coupled thermoelasticity. *Comput Struct*, 31(1):73–80, 1989.

[20] SY Chen, MS Ju, and YG Tsuei. Estimation of mass, stiffness and damping matrices from frequency response functions. *J Vib Acoust*, 118(1):78–82, 1996.

[21] B Cockburn, G E Karniadakis, and C-W Shu. The development of discontinuous Galerkin methods. In *Discontinuous Galerkin Methods*, pages 3–50. Springer, 2000.

[22] C Demain, M Journée, and C Bertrand. Evaluation of different models to estimate the global solar radiation on inclined surfaces. *Renew Energ*, 50:710–721, 2013.

[23] R S Esfandiari. *Numerical methods for engineers and scientists using MATLAB®*. Crc Press, 2017.

[24] L Evangelisti, C Guattari, F Asdrubali, and R de Lieto Vollaro. An experimental investigation of the thermal performance of a building solar shading device. *J Build Eng*, 28:101089, 2020.

[25] J Fageot, S Aziznejad, M Unser, and V Uhlmann. Support and approximation properties of Hermite splines. *J Comput Appl Math*, 368:112503, 2020.

[26] P Foraboschi. Buckling of a laminated glass column under test. *Struct Eng*, 87(1):2–8, 2009.

[27] P Foraboschi. Analytical modeling to predict thermal shock failure and maximum temperature gradients of a glass panel. *Mater Des*, 134:301–319, 2017.

[28] C Frey, S Dölling, M Leštáková, and W Becker. Free-edge crack onset induced by thermal loading. *Int J Sol Struct*, 230:111160, 2021.

[29] Thomas-Peter Fries and Ted Belytschko. The extended/generalized finite element method: an overview of the method and its applications. *International journal for numerical methods in engineering*, 84(3):253–304, 2010.

[30] L Galuppi, M Maffeis, and G Royer-Carfagni. Enhanced engineered calculation of the temperature distribution in architectural glazing exposed to solar radiation. *Glass Struct Eng*, 6(4):425–448, 2021.

[31] L Galuppi, M Maffeis, and G Royer-Carfagni. Engineered calculation of the uneven in-plane temperatures in Insulating Glass Units for structural design. *Glass Struct Eng,* https://doi.org/10.1007/s40940-022-00169, 2022.

[32] B E Gatewood. *Thermal Stresses*. McGraw–Hill Publication in Aeronautical Science, 1957.

[33] S L Guo, B L Wang, K F Wang, and J E Li. Coupling effects of dual-phase-lag heat conduction and property difference on thermal shock fracture of coating/substrate structures. *Int J Sol Struct*, 152:238–247, 2018.

[34] M Hermanns, F del Ama, and J A Hernández. Analytical solution to the one-dimensional non-uniform absorption of solar radiation in uncoated and coated single glass panes. *Energy Build*, 47:561–571, 2012.

[35] T JR Hughes. *The finite element method: linear static and dynamic finite element analysis*. Courier Corporation, 2012.

[36] K A R Ismail and J R Henriquez. Modeling and simulation of a simple glass window. *Sol Energ Mat Sol C*, 80(3):355–374, 2003.

[37] AW Lang and DM Sloan. Hermite collocation solution of near-singular problems using numerical coordinate transformations based on adaptivity. *Journal of computational and applied mathematics*, 140(1-2):499–520, 2002.

[38] T J Lardner. Biot's variational principle in heat conduction. *AIAA Journal*, 1(1):196–206, 1963.

[39] Q H Li and J Wang. Weak Galerkin finite element methods for parabolic equations. *Numerical Methods for Partial Differential Equations*, 29(6):2004–2024, 2013.

[40] J H IV Lienhard and J H V Lienhard. *A heat transfer textbook, 5th edition*. Phlogiston press, 2019.

[41] D Liu, X Zheng, and Y Liu. A discontinuous Galerkin finite element method for heat conduction problems with local high gradient and thermal contact resistance. *Computer Modeling in Engineering and Sciences (CMES)*, 39(3):263, 2009.

[42] A E H Love. *A treatise on the mathematical theory of elasticity*. Cambridge university press, 2013.

[43] H Manz, S Brunner, and L Wullschleger. Triple vacuum glazing: Heat transfer and basic mechanical design constraints. *Sol Energy*, 80(12):1632–1642, 2006.

[44] C Marino, A Nucara, M Pietrafesa, and E Polimeni. The effect of the short wave radiation and its reflected components on the mean radiant temperature: modelling and preliminary experimental results. *J Build Eng*, 9:42–51, 2017.

[45] MATLAB. *version R200a - academic use*. The MathWorks Inc., Natick, Massachusetts, 2020.

[46] D J Norris. Solar radiation on inclined surfaces. *Sol Energy*, 10(2):72–76, 1966.

[47] P O'Hara, CA Duarte, and T Eason. A two-scale generalized finite element method for interaction and coalescence of multiple crack surfaces. *Engineering Fracture Mechanics*, 163:274–302, 2016.

[48] M Poláková, S Schäfer, and M Elstner. Thermal glass stress analysis–design considerations. In *Challenging Glass Conference Proceedings*, volume 6, pages 725–740, 2018.

[49] R Powles, D Curcija, and C Kohler. Solar absorption in thick and multilayered glazings. In *Proceedings of World Renewable Energy Congress VII*, 2002.

[50] William H Reed and Thomas R Hill. Triangular mesh methods for the neutron transport equation. Technical report, Los Alamos Scientific Lab., N. Mex.(USA), 1973.

[51] C S Rekatsinas and D A Saravanos. A cubic spline layerwise time domain spectral FE for guided wave simulation in laminated composite plate structures with physically modeled active piezoelectric sensors. *Int J Sol Struct*, 124:176–191, 2017.

[52] K Shye and M Richardson. Mass, stiffness, and damping matrix estimates from structural measurements. In *Proceedings of the 5th International Modal Analysis Conference*, volume 1, pages 756–761. Citeseer, 1987.

[53] D Stahn. Thermal stresses in heat-absorbing building glass subjected to solar radiation. In *Thermal Stresses in Severe Environments*, pages 305–323. Springer, 1980.

[54] C S Strobel, M O Abadie, and N Mendes. Absorption of solar radiation in thick and multilayered glazing. In *Building Simulation 2007 Conference, Beijing, China*, 2007.

[55] Theofanis Strouboulis, Kevin Copps, and Ivo Babuška. The generalized finite element method. *Computer methods in applied mechanics and engineering*, 190(32-33):4081–4193, 2001.

[56] W C Swinbank. Long-wave radiation from clear skies. *Q J Roy Meteor Soc*, 89(381):339–348, 1963.

[57] T Szabó. On the discretization time-step in the finite element theta-method of the discrete heat equation. In *International Conference on Numerical Analysis and Its Applications*, pages 564–571. Springer, 2008.

[58] K Vengatesan. Windows Film to Glass: Numerical simulation software for avoiding thermal stress. MS Thesis, IST Tecnico Lisboa, 2017.

[59] B Vujanovic. Application of the optimal linearization method to the heat transfer problem. *Int J Heat and Mass Transf*, 16(6):1111–1117, 1973.

[60] J L Wright. Calculating center-glass performance indices of windows. *ASHRAE Trans*, 104:1230–1241, 1998.

[61] O C Zienkiewicz, R L Taylor, P Nithiarasu, and J Z Zhu. *The finite element method*, volume 3. McGraw-hill London, 1977.

A Explicit matrix expressions

A.1 Connectivity matrices

Explicit expressions for the connectivity matrices $\mathbf{L}_i$ appearing in eq. (3.26) are

$$\mathbf{L}_1 := \begin{bmatrix} 1 & 0 & 0 & 0 & 0 & \dots & 0 & \dots & 0 \\ 0 & 1 & 0 & 0 & 0 & \dots & 0 & \dots & 0 \\ 0 & 0 & 1 & 0 & 0 & \dots & 0 & \dots & 0 \\ 0 & 0 & 0 & 1 & 0 & \dots & 0 & \dots & 0 \\ 0 & 0 & 0 & 0 & 0 & \dots & 1 & \dots & 0 \end{bmatrix}, \qquad \text{(A.1)}$$

$(2N+3)$th column

$$\mathbf{L}_2 := \begin{bmatrix} 0 & \beta_{1;2} & 0 & 0 & 0 & 0 & \dots & 0 & \dots & 0 \\ 0 & 0 & 0 & 0 & 1 & 0 & \dots & 0 & \dots & 0 \\ 0 & 0 & 0 & \beta_{1;2}\gamma_{1;2} & 0 & 0 & \dots & 0 & \dots & 0 \\ 0 & 0 & 0 & 0 & 0 & 1 & \dots & 0 & \dots & 0 \\ 0 & 0 & 0 & 0 & 0 & 0 & \dots & 1 & \dots & 0 \end{bmatrix}, \qquad \text{(A.2)}$$

$(2N+4)$th column

$$\mathbf{L}_i := \begin{bmatrix} 0 & \dots & 0 & \beta_{i;i+1} & 0 & 0 & 0 & \dots & 0 & \dots & 0 \\ 0 & \dots & 0 & 0 & 0 & 1 & 0 & \dots & 0 & \dots & 0 \\ 0 & \dots & 0 & 0 & \beta_{i;i+1}\gamma_{i;i+1} & 0 & 0 & \dots & 0 & \dots & 0 \\ 0 & \dots & 0 & 0 & 0 & 0 & 1 & \dots & 0 & \dots & 0 \\ 0 & \dots & 0 & 0 & 0 & 0 & 0 & \dots & 1 & \dots & 0 \end{bmatrix}, \qquad \text{(A.3)}$$

$\underbrace{}_{2(i-1)}$ $(2N+2+i)$th column

where $\beta_{i;i+1}$ and $\gamma_{i;i+1}$ are defined by (3.24).
Notice that, when $N = 1$, matrix $\mathbf{L}_1$ reduces to a 5×5 identity matrix.

A.2 "Stiffness" and "damping" matrices

Explicit matrix expressions for $\mathbf{K}$ and $\mathbf{C}'$ appearing in eq.s (3.30) and (3.31), respectively, are

$$\mathbf{K} := \int_0^1 [\mathbf{p}(\zeta)\ \mathbf{p}(\zeta)]\ d\zeta = \begin{bmatrix} \frac{13}{35} & \frac{9}{70} & \frac{11}{210} & -\frac{13}{420} & 0 \\ \frac{9}{70} & \frac{13}{35} & \frac{13}{420} & -\frac{11}{210} & 0 \\ \frac{11}{210} & \frac{13}{420} & \frac{1}{105} & -\frac{1}{140} & 0 \\ -\frac{13}{420} & -\frac{11}{210} & -\frac{1}{140} & \frac{1}{105} & 0 \\ 0 & 0 & 0 & 0 & 0 \end{bmatrix}, \tag{A.4}$$

$$\mathbf{C}' := \int_0^1 [\mathbf{n}(\zeta)\ \mathbf{n}(\zeta)]\ d\zeta = \begin{bmatrix} \frac{23}{504} & -\frac{1}{252} & \frac{19}{2016} & \frac{11}{10080} & -\frac{3}{20} \\ -\frac{1}{252} & \frac{23}{504} & -\frac{11}{10080} & -\frac{19}{2016} & \frac{3}{20} \\ \frac{19}{2016} & -\frac{11}{10080} & \frac{1}{504} & \frac{1}{3360} & -\frac{1}{30} \\ \frac{11}{10080} & -\frac{19}{2016} & \frac{1}{3360} & \frac{1}{504} & \frac{1}{30} \\ -\frac{3}{20} & \frac{3}{20} & -\frac{1}{30} & \frac{1}{30} & 1 \end{bmatrix}. \tag{A.5}$$

Explicit matrix expressions for $\mathbf{C}''_{int}$ and $\mathbf{C}''_{ext}$ appearing in eq. (3.34) are

$$\mathbf{C}''_{int} := \mathbf{n}(1)\mathbf{n}^T(1) = \begin{bmatrix} 0 & 0 & 0 & 0 & 0 \\ 0 & \frac{1}{4} & 0 & -\frac{1}{24} & \frac{1}{2} \\ 0 & 0 & 0 & 0 & 0 \\ 0 & -\frac{1}{24} & 0 & \frac{1}{144} & -\frac{1}{12} \\ 0 & \frac{1}{2} & 0 & -\frac{1}{12} & 1 \end{bmatrix}, \tag{A.6}$$

$$\mathbf{C}''_{ext} := \mathbf{n}(0)\mathbf{n}^T(0) = \begin{bmatrix} \frac{1}{4} & 0 & \frac{1}{24} & 0 & -\frac{1}{2} \\ 0 & 0 & 0 & 0 & 0 \\ \frac{1}{24} & 0 & \frac{1}{144} & 0 & -\frac{1}{12} \\ 0 & 0 & 0 & 0 & 0 \\ -\frac{1}{2} & 0 & -\frac{1}{12} & 0 & 1 \end{bmatrix}. \tag{A.7}$$

Explicit expressions for matrices $\mathbf{M}_1 =$ and $\mathbf{M}_0$ appearing in eq. (3.35) are

$$\mathbf{M}_1 := \mathbf{n}(1)\mathbf{p}^T(1) = \begin{bmatrix} 0 & 0 & 0 & 0 & 0 \\ 0 & \frac{1}{2} & 0 & 0 & 0 \\ 0 & 0 & 0 & 0 & 0 \\ 0 & -\frac{1}{12} & 0 & 0 & 0 \\ 0 & 1 & 0 & 0 & 0 \end{bmatrix}, \tag{A.8}$$

$$\mathbf{M}_0 := \mathbf{n}(0)\mathbf{p}^T(0) = \begin{bmatrix} 0 & -\frac{1}{2} & 0 & 0 & 0 \\ 0 & 0 & 0 & 0 & 0 \\ 0 & -\frac{1}{12} & 0 & 0 & 0 \\ 0 & 0 & 0 & 0 & 0 \\ 0 & 1 & 0 & 0 & 0 \end{bmatrix}. \tag{A.9}$$

Vectors $\mathbf{n}(0)$ and $\mathbf{n}(1)$, allowing to evaluate terms $\tilde{\mathbf{b}}(t)$ and $\mathbf{b}^+(t)$ appearing in eq. (3.37), are

$$\mathbf{n}(0) = \begin{bmatrix} -\frac{1}{2} \\ 0 \\ -\frac{1}{12} \\ 0 \\ 1 \end{bmatrix}, \quad \mathbf{n}(1) = \begin{bmatrix} 0 \\ \frac{1}{2} \\ 0 \\ -\frac{1}{12} \\ 1 \end{bmatrix}. \tag{A.10}$$

The explicit expression for vector $\mathbf{a} := \int_0^1 \zeta \mathbf{n}(\zeta)\, d\zeta$ appearing in eq. (3.39) is

$$\mathbf{a} := \int_0^1 \zeta \mathbf{n}(\zeta)\, d\zeta = \begin{bmatrix} -\frac{1}{30} \\ \frac{7}{60} \\ -\frac{1}{120} \\ -\frac{1}{40} \\ \frac{1}{2} \end{bmatrix}. \tag{A.11}$$